J. Fluid Mech. (2017), *vol.* 824, *pp.* 477–512.
doi:10.1017/jfm.2017.350

Generalized rapid-distortion theory on transversely sheared mean flows with physically realizable upstream boundary conditions: application to trailing-edge problem

M. E. Goldstein[1,†], S. J. Leib[2] and M. Z. Afsar[3]

[1]National Aeronautics and Space Administration, Glenn Research Center, Cleveland, OH 44135, USA

[2]Ohio Aerospace Institute, Cleveland, OH 44142, USA

[3]Department of Mechanical and Aerospace Engineering, Strathclyde University, 75 Montrose St., Glasgow GI 1XJ, UK

(Received 9 February 2017; revised 16 May 2017; accepted 18 May 2017; first published online 6 July 2017)

This paper is concerned with rapid-distortion theory on transversely sheared mean flows which (among other things) can be used to analyse the unsteady motion resulting from the interaction of a turbulent shear flow with a solid surface. It extends previous analyses of Goldstein *et al.* (*J. Fluid Mech.*, vol. 736, 2013*a*, pp. 532–569; *NASA/TM*-2013-217862, 2013*b*) which showed that the unsteady motion is completely determined by specifying two arbitrary convected quantities. The present paper uses a pair of previously derived conservation laws to derive upstream boundary conditions that relate these quantities to experimentally measurable flow variables. The result is dependent on the imposition of causality on an intermediate variable that appears in the conservation laws. Goldstein *et al.* (2013*a*) related the convected quantities to the physical flow variables at the location of the interaction, but the results were not generic and hard to reconcile with experiment. That problem does not occur in the present formulation, which leads to a much simpler and more natural result than the one given in Goldstein *et al.* (2013*a*). We also show that the present formalism yields better predictions of the sound radiation produced by the interaction of a two-dimensional jet with the downstream edge of a flat plate than the Goldstein *et al.* (2013*a*) result. The role of causality is also discussed.

Key words: aeroacoustics, mathematical foundations, turbulent flows

1. Introduction

Rapid-distortion theory (RDT) uses linear analysis to study the interaction of turbulence with solid surfaces. It applies whenever the turbulence intensity is small and the length (or time) scale over which the interaction takes place is short compared to the length (or time) scale over which the turbulent eddies evolve (Hunt 1973;

† Email address for correspondence: Marvin.E.Goldstein@nasa.gov

Goldstein 1978*a*, 1979*a*). When interpreted asymptotically, these assumptions imply, among other things, that it is possible to identify a distance that is very (infinitely) large on the scale of the interaction, but still small on the scale over which the turbulent eddies evolve. The assumptions also imply that the resulting flow is inviscid and non-heat-conducting and is, therefore, governed by the linearized Euler equations, i.e. the Euler equations linearized about an arbitrary, usually steady, solution to the nonlinear equations – customarily referred to as the base flow.

The simplest case occurs when the base flow is completely uniform. In his now classical paper, Kovasznay (1953) showed that the unsteady isentropic motion on this flow can be decomposed into the sum of a vortical disturbance that has no pressure fluctuations and an irrotational disturbance that carries the pressure fluctuations. The latter satisfies a second-order wave equation when the flow is compressible, and should either decay or propagate relative to the base flow. It can, therefore, be associated with the acoustic component of the motion on these flows. The former, which moves downstream at the mean flow velocity, i.e. it is a purely convected quantity, can be associated with the remaining, hydrodynamic, component of the motion. Any convected velocity field will satisfy the linearized momentum equations for this flow, but continuity only allows two of its components to be arbitrary. These two quantities can then be independently specified as time-stationary boundary conditions for unsteady surface interaction problems. This makes the Kovasznay decomposition particularly useful for analysing problems that involve the interaction of turbulence (which corresponds to the hydrodynamic component of the motion) with surfaces embedded in uniform mean flows (Sears 1941), or in flows that become uniform in the upstream region (Hunt 1973; Goldstein 1978*a*, 1979*a*). It is worth noting, however, that the Kovasznay decomposition is not unique because there are irrotational (homogeneous) solutions that carry no pressure fluctuations and can therefore be associated with either the vortical component or with the irrotational component.

There have been a number of attempts to extend these ideas to non-uniform base flows, but the situation is considerably more complicated when the entire base flow is non-uniform. The simplest case occurs when the base flow U is incompressible and the mean shear is uniform, i.e.

$$U = \gamma y_2, \tag{1.1}$$

where γ is a constant and y_1, y_2, y_3 are Cartesian coordinates, with y_1 being in the mean flow direction. Then the two-dimensional small-amplitude motion is determined by the linearized incompressible vorticity equation, $(\partial/\partial\tau + U\partial/\partial y_1)\omega_3' = 0$, where τ denotes the time and ω_3' the two-dimensional spanwise vorticity perturbation. Orr (1907, see also Drazin & Reid 1981, pp. 147–151) pointed out that this equation or, equivalently, the two-dimensional Rayleigh equation

$$\frac{\partial}{\partial y_1}\left(\frac{\partial}{\partial\tau} + U\frac{\partial}{\partial y_1}\right)\omega_3' = \left(\frac{\partial}{\partial\tau} + U\frac{\partial}{\partial y_1}\right)\left(\frac{\partial^2}{\partial y_1^2} + \frac{\partial^2}{\partial y_2^2}\right)v_2' = 0, \tag{1.2}$$

which determines the unsteady cross-gradient velocity perturbation $v_2'(y_2, \tau)$ can be integrated to obtain

$$\left(\frac{\partial^2}{\partial y_1^2} + \frac{\partial^2}{\partial y_2^2}\right)v_2' = \frac{\partial}{\partial y_1}\omega_c\left(\tau - \frac{y_1}{\gamma y_2}, y_2\right), \tag{1.3}$$

where the imposed spanwise vorticity perturbation ω_3', which we denote by ω_c, can be an arbitrary function of its arguments. Orr (1907) obtained an analytic

solution to an initial value problem associated with this equation and used it to study the development of the velocity and pressure fluctuations starting from some initial state. But the long-time solutions to at least some initial value problems are likely to develop internal shear layers that can no longer be considered inviscid and are susceptible to Kelvin–Helmholtz instabilities (Brinkman & Walker 2001; Cowley 2001; Cassel & Conlisk 2014), and are therefore not necessarily relevant to the time-stationary turbulent flows being considered here. It does, however, seem reasonable to use the steady state (i.e. time stationary) solutions of this equation to represent the turbulence in these flows. The solutions will then be of the form

$$v_2'(\boldsymbol{x}, t) = \frac{\partial}{\partial x_1} \int_{-T}^{T} \int g_0(\boldsymbol{x}, t \,|\, \boldsymbol{y}, \tau) \omega_c \left(\tau - \frac{y_1}{\gamma y_2}, y_2 \right) \mathrm{d}\boldsymbol{y} \, \mathrm{d}\tau, \tag{1.4}$$

where $\boldsymbol{x} = \{x_1, x_2\}$, $\boldsymbol{y} = \{y_1, y_2\}$ denote the two-dimensional Cartesian coordinates, T denotes a large time interval and g_0 is a two-dimensional Green's function that satisfies the Poisson equation

$$\left(\frac{\partial^2}{\partial x_1^2} + \frac{\partial^2}{\partial x_2^2} \right) g_0(\boldsymbol{x}, t \,|\, \boldsymbol{y}, \tau) = \delta(t - \tau) \delta(\boldsymbol{y} - \boldsymbol{x}). \tag{1.5}$$

The vorticity ω_3', which is equal to the convected quantity $\omega_c(\tau - y_1/U(y_2), y_2)$, can now be specified as a boundary condition since (1.4) will satisfy (1.3) for any choice of this quantity. The inner integral in (1.4) will be over a bounded or semibounded region of space, with the Green's function g_0 chosen to satisfy appropriate transverse boundary conditions when solid surfaces are present in the flow, and the integral will be over all space and g_0 can therefore be taken to be $(4\pi)^{-1} \ln |\boldsymbol{x} - \boldsymbol{y}|^2 \delta(t - \tau)$ when they are not. The transverse velocity perturbation $v_2'(\boldsymbol{x}, t)$ would then be given by (see Gradshteyn & Ryshik 1965, p. 406 #3.723)

$$v_2'(\boldsymbol{x}, t) = \int_{-\infty}^{\infty} \bar{G}_0(x_2 \,|\, y_2) \omega_c(t - x_1/\gamma y_2) \, \mathrm{d}y_2, \tag{1.6}$$

with

$$\bar{G}_0(x_2 \,|\, y_2) \equiv \frac{\mathrm{i}}{2} (\operatorname{sgn} \omega)(\operatorname{sgn} y_2) \mathrm{e}^{-|\omega||x_2 - y_2|/\gamma |y_2|} \tag{1.7}$$

when the convected vorticity $\omega_c(t - y_1/U(y_2), y_2)$ is taken to be the generic time-harmonic function

$$\omega_c \left(t - \frac{y_1}{U(y_2)}, y_2 \right) = \mathrm{e}^{\mathrm{i}\omega[t - y_1/U(y_2)]} \tilde{\Omega}_c(y_2 : \omega), \tag{1.8}$$

which can be summed over frequency to represent an arbitrary-time-dependent flow. Some typical results for the transverse velocity perturbation resulting from (1.8) with $\tilde{\Omega}_c(y_2 : \omega)$ taken to be

$$\tilde{\Omega}_c(y_2 : \omega) = \mathrm{e}^{-[a(y_2 - y_0)]^2} \tag{1.9}$$

are plotted in figure 1, which shows that this quantity differs from its purely convected counterpart on a uniform mean flow in that it now decays as $x_1 \to \pm\infty$.

Similar behaviour is also expected to occur in surface interaction problems, which might, for example, involve placing a leading edge at $y_1 = 0$ (see figure 2). This

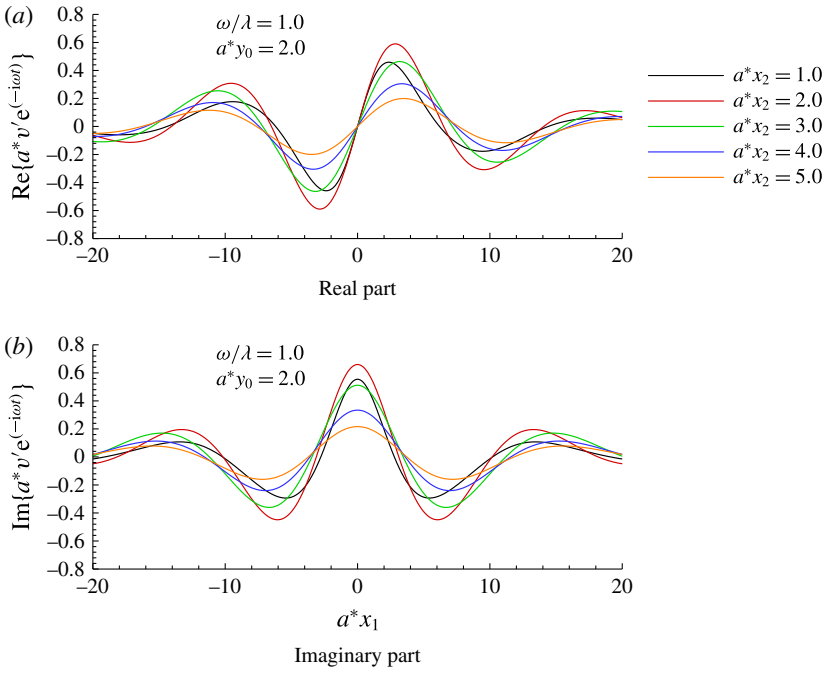

FIGURE 1. Cross-gradient velocity fluctuations produced by the convected vorticity (1.8) for the indicated values of the parameters.

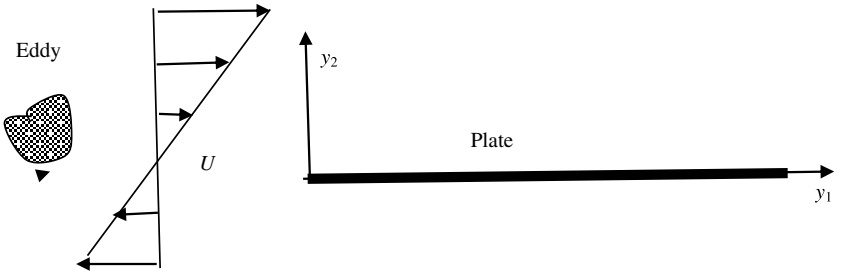

FIGURE 2. Leading-edge scattering.

implies that the upstream boundary conditions cannot be imposed by simply specifying v_2' at upstream infinity when constructing solutions to these types of problems.

But (1.3) shows that the Laplacian of the cross-gradient velocity v_2' is equal to the streamwise derivative of the convected quantity $\omega_c(\tau - y_1/U(y_2), y_2)$ and, therefore, does not decay, which means that it can be specified infinitely far upstream on the length scale over which the interaction takes place, which, as noted above, can be still asymptotically small compared to the scale over which the turbulent eddies evolve. The important point is that the arbitrary convected quantity $\omega_c(\tau - y_1/U(y_2), y_2)$ can be determined by specifying an appropriate experimentally measurable quantity in a region of the flow that is uninfluenced by the rapid-distortion interaction. Not surprisingly, the situation is somewhat more complex for arbitrary transversely sheared mean flows, which is further complicated by the need to consider causality. The focus of this paper is on extending these ideas to such flows and using the results to specify

appropriate upstream boundary conditions for RDT problems on these more general mean flows.

Equation (1.3) was extended to three-dimensional compressible motions on general transversely sheared mean flows by Goldstein (1978*b*, 1979*b*) (hereafter referred to as G78 and G79, respectively) and Goldstein, Afsar & Leib (2013*a*) (hereafter referred to as GAL) – who showed how their more general results can be used to formulate RDT problems that are relevant to aircraft-noise prediction. Their results can be thought of as a natural generalization of the Kovasznay (1953) decomposition in that the general formalism developed in those references, which is summarized in § 2 of the current paper, shows that the bounded solutions to the linearized Euler equations governing the small-amplitude motion on a transversely sheared mean flow involve two purely convected quantities that can be arbitrarily specified as input conditions. But these quantities must be related to physically measurable flow variables in order to obtain solutions that can be compared with experiment. GAL obtained the required relations by assuming that they would be the same as those that would exist at the location of the scattering inhomogeneity in a streamwise-homogeneous flow (that would exist in the absence of any scattering inhomogeneities in the streamwise direction). The result was quite complicated (and ultimately had to be approximated) and, more importantly, required that the physical variables be measured in a different flow from the one being analysed. As noted above, a major purpose of the present paper is to relate the convected quantities to the physical variables in a way that does not exhibit any of these drawbacks by imposing appropriate upstream boundary conditions in the undisturbed region of the flow being analysed – as was done in G78 and G79. The present paper generalizes and extends these results and shows by example that this leads to considerably improved agreement with experiment.

There are a large number of papers (e.g. Taylor 1935; Batchelor & Proudman 1954; Livescu & Madnia 2004; Sagaut & Cambon 2008; Xie, Karimi & Girimaji 2017 and references therein) that use locally homogeneous RDT (which is a kind of local high-frequency approximation) first introduced by Moffatt (1967) to study the unsteady motion on planar sheared flows (see Moffatt 1967). But the local nature of this approximation obviates the need to consider the upstream boundary condition issue, which is arguably the main focus of this paper. More general global solutions can be obtained by using non-homogeneous RDT, which usually provides a more realistic representation of the turbulence but requires the imposition of upstream boundary conditions. Hunt (1973) used non-homogeneous RDT to study the distortion of turbulence by an irrotational base flow.

Early work on RDT was restricted to incompressible flows. Goldstein (1978*a*) and G79 introduced compressibility effects into the (more general non-homogeneous) theory, which allowed the inclusion of an acoustic as well as a vortical component of the motion (as in the Kovasznay 1953 decomposition) and not just a vortical component. But more importantly, the inclusion of compressibility enabled the application of RDT to the prediction of the radiated sound field produced by the flow. GAL used the compressible theory developed in G79 to predict the sound radiation produced by the interaction of a two-dimensional jet with the downstream edge of a flat plate. They employed low-frequency asymptotics to obtain a relatively simple explicit formula and used it to predict the radiated sound field. The results were in reasonable agreement with data, but the high-frequency roll-off of the predicted spectrum tended to be much slower than the experimental results. The present paper shows that this deficiency can be corrected by considering the high-frequency limit. We again obtain an explicit formula for the radiated sound field that reduces to

the GAL result when one of its factors is set equal to unity. But this factor also approaches unity when the appropriately scaled frequency parameter approaches zero so that the result behaves like a uniformly valid composite solution that applies at all frequencies. The predictions based on this formula are found to be in much better agreement with the experiments than those given in GAL.

While GAL and the present paper use the same application to illustrate the general formalism (i.e. the interaction of a two-dimensional jet with the downstream edge of a flat plate) the improved relations between the theoretical convected quantities and the measurable flow variables makes the present results applicable to a wide range of flow–surface interaction problems. Examples include analysis of more complicated geometries, such as deformable plates inclined to the mean flow (Chinaud *et al.* 2014), which could be of interest in optimization studies for reducing edge-generated noise.

Linear theories are also used to study the shock–turbulence interaction and are often referred to as linear interaction approximations (LIA) in this context (see for example, Ribner (1953), Moore (1954), Woushuk *et al.* (2009, 2012), Huete *et al.* (2011, 2012) as well as extensive discussion of the subject by Sagaut & Cambon (2008)). Compressible RDT and LIA share some common features. Both approaches decompose the flow into acoustic and vortical components and both use Fourier and/or Laplace transforms to eliminate the time dependence.

The paper begins by briefly summarizing the results obtained in GAL for the formal solution to the complete inhomogeneous RDT problem. As in G78 and G79, the unsteady motion is determined by two convected quantities that can be arbitrarily specified as boundary (or initial) conditions. But, as noted above, it is necessary to link these quantities to physical (preferably measurable) flow variables in order to relate the solution to conditions that can be controlled by the experimentalist. Conservation laws that relate the convected quantities, physical variables and transverse particle displacement are summarized in § 3. Section 4 discusses the implications of imposing causality on the solution and shows that the transverse particle displacement defined in § 3 vanishes at upstream infinity when this condition is imposed. Section 5 shows that the result for the transverse particle displacement can be inserted into these conservation laws to obtain an appropriate set of upstream boundary conditions that link the arbitrary convected quantities to the physical flow variables. Section 6 shows how the Fourier transforms of these boundary conditions can be used to relate the spectra of the convected quantities to the spectra of the physical variables that would actually be measured in an experiment. The results are then used to obtain a formula for the sound radiation produced by the interaction of a two-dimensional jet with the trailing edge of a flat plate that extends the result derived in GAL. The formula is used to obtain numerical predictions that are compared with data taken at NASA Glenn Research Center (Zaman, Brown & Bridges 2013; Bridges, Brown & Bozak 2014; Brown 2015) as part of a large experimental campaign to study jet–surface interaction noise (Brown 2012; Bridges 2014). The comparisons were carried out over a broader range of parameters than those in GAL, and the agreement is now significantly improved relative to those results. The solution is also used to discuss the effects of imposing causality.

2. Review of basic formalism and comparison with the Orr result

As in G78, G79 and GAL the flow is assumed to be inviscid and non-heat-conducting and the fluid is assumed to be an ideal gas so that the entropy is proportional to $\ln(p/\rho^{\gamma})$ and the squared sound speed is equal to $\gamma p/\rho$, where p

denotes the pressure, ρ the density and γ the specific heat ratio. Then the pressure $p' = p - p_0$ and mass flux

$$u_i \equiv \rho v_i', \tag{2.1}$$

perturbations (where v_i' denotes the velocity perturbation) on a transversely sheared mean flow with pressure $p_0 = \text{const.}$, velocity $U(\boldsymbol{y}_T)$ and mean sound speed squared $c^2(\boldsymbol{y}_T)$, are governed by the linearized Euler equations

$$\frac{\mathrm{D}_0 u_i}{\mathrm{D}\tau} + \delta_{1i} u_j \frac{\partial U}{\partial y_j} + \frac{\partial}{\partial y_i} p' = 0 \tag{2.2}$$

and

$$\frac{\mathrm{D}_0 p'}{\mathrm{D}\tau} + \frac{\partial}{\partial y_j} c^2 u_j = 0, \tag{2.3}$$

where $\boldsymbol{y}_T = \{y_2, y_3\}$, $\boldsymbol{y} = \{y_1, y_2, y_3\} = \{y_1, \boldsymbol{y}_T\}$ and $\mathrm{D}_0/\mathrm{D}\tau \equiv \partial/\partial\tau + U\partial/\partial y_1$ denotes the convective derivative.

G79 shows that the solution to these equations can be expressed in terms of the two arbitrary convected functions $\tilde{\omega}_c(\tau - y_1/U, \boldsymbol{y}_T)$ and $\vartheta(\tau - (y_1/U), \boldsymbol{y}_T)$ and a potential function ϕ that satisfies

$$L_a \phi = -\tilde{\omega}_c \left(\tau - \frac{y_1}{U}, \boldsymbol{y}_T\right), \tag{2.4}$$

where

$$L_a \equiv \frac{\mathrm{D}_0^3}{\mathrm{D}\tau^3} - \frac{\partial}{\partial y_i} c^2 \left(\frac{\partial}{\partial y_i}\frac{\mathrm{D}_0}{\mathrm{D}\tau} + 2\frac{\partial U}{\partial y_i}\frac{\partial}{\partial y_1}\right) \tag{2.5}$$

and the physical variables p' and u_i are determined by

$$p' = -\frac{\mathrm{D}_0^3 \phi}{\mathrm{D}\tau^3}, \tag{2.6}$$

and

$$u_i = \left(\delta_{ij}\frac{\mathrm{D}_0}{\mathrm{D}\tau} - \delta_{i1}\frac{\partial U}{\partial y_j}\right)\lambda_j + \varepsilon_{ijk}\frac{1}{c^2}\frac{\partial U}{\partial y_j}\frac{\partial}{\partial y_k}\vartheta\left(\tau - \frac{y_1}{U}, \boldsymbol{y}_T\right), \tag{2.7}$$

with δ_{ij} denoting the Kronecker delta, ε_{ijk} the alternating tensor and

$$\lambda_j \equiv \frac{\partial}{\partial y_j}\frac{\mathrm{D}_0 \phi}{\mathrm{D}\tau} + 2\frac{\partial U}{\partial y_j}\frac{\partial \phi}{\partial y_1} \tag{2.8}$$

denoting a kind of generalized particle displacement.

It is well known that the mass flux perturbation, u_i, can be eliminated between (2.2) and (2.3) to show that the pressure fluctuation p' satisfies Rayleigh's equation

$$Lp' = 0, \tag{2.9}$$

where

$$L \equiv \frac{\mathrm{D}_0}{\mathrm{D}\tau}\left(\frac{\partial}{\partial y_i} c^2 \frac{\partial}{\partial y_i} - \frac{\mathrm{D}_o^2}{\mathrm{D}\tau^2}\right) - 2\frac{\partial U}{\partial y_j}\frac{\partial}{\partial y_1} c^2 \frac{\partial}{\partial y_j} \tag{2.10}$$

denotes the usual Rayleigh operator, which is easily shown to be adjoint to the operator L_a.

For reasons given in the introduction, our focus here is on the steady state (i.e. time stationary) solutions (which are assumed to exist) and we suppose that ϕ is a stationary random function (Wiener 1938) and therefore that initial conditions imposed in the distant past have all decayed out at the finite time t. A formal steady state solution to (2.4) can then be written as

$$\phi(\boldsymbol{x},t) = -\int_{-T}^{T}\int_{V} g(\boldsymbol{y},\tau\,|\,\boldsymbol{x},t)\tilde{\omega}_c\left(\tau-\frac{y_1}{U(\boldsymbol{y}_T)},\boldsymbol{y}_T\right)\mathrm{d}\boldsymbol{y}\,\mathrm{d}\tau + \int_{-T}^{T}\int_{S}\hat{n}_j c^2\left[g(\boldsymbol{y},\tau\,|\,\boldsymbol{x},t)\lambda_j - \frac{\partial g(\boldsymbol{y},\tau\,|\,\boldsymbol{x},t)}{\partial y_j}\frac{\mathrm{D}_0\phi}{\mathrm{D}\tau}\right]\mathrm{d}S(\boldsymbol{y})\,\mathrm{d}\tau, \quad (2.11)$$

where $g(\boldsymbol{y},\tau\,|\,\boldsymbol{x},t)$ denotes the Rayleigh operator Green's function which exhibits incoming wave behaviour as $|\boldsymbol{y}|\to\infty$ and satisfies

$$Lg(\boldsymbol{y},\tau\,|\,\boldsymbol{x},t)=\delta(\boldsymbol{y}-\boldsymbol{x})\delta(\tau-t), \quad (2.12)$$

the first two arguments of $g(\boldsymbol{y},\tau\,|\,\boldsymbol{x},t)$ denote the dependent variables and the second two denote the source variables, T denotes a very large but finite time interval, V is a region of space bounded by cylindrical (i.e. parallel to the mean flow) surface(s) S that can be finite, semi-infinite or infinite in the streamwise direction and $\hat{\boldsymbol{n}}=\{\hat{n}_i\}$ is the unit outward-drawn normal to S. The upper limit $+T$ of the τ-integration can be replaced by t since $g(\boldsymbol{y},\tau\,|\,\boldsymbol{x},t)=0$ for $\tau>t$. The lower limit $-T$ reflects the fact that the initial conditions must be imposed in the distant past in order to ensure that they do not contribute to the steady state solution.

Equation (2.11) expresses the solution to (2.4) in terms of the volume source distribution $\tilde{\omega}_c(\tau-y_1/U(\boldsymbol{y}_T),\boldsymbol{y}_T)$ and the values of the potential ϕ on some arbitrary cylindrical surfaces S (some or all of which may be at infinity). The analysis is somewhat unconventional in that the direct Green's function g now plays the role of an adjoint Green's function for the solution ϕ.

The surface integrals in (2.11) drop out when any of the surfaces S are at infinity (i.e. when V represents all of space) and they can be eliminated when they are not by requiring that the Green's function g satisfies certain boundary conditions on these bounding surfaces (since g is not uniquely determined by (2.12)). Equation (2.11) then becomes

$$\phi(\boldsymbol{x},t)=-\int_{-T}^{T}\int_{V} g(\boldsymbol{y},\tau\,|\,\boldsymbol{x},t)\tilde{\omega}_c\left(\tau-\frac{y_1}{U(\boldsymbol{y}_T)},\boldsymbol{y}_T\right)\mathrm{d}\boldsymbol{y}\,\mathrm{d}\tau. \quad (2.13)$$

Equations (2.6) and (2.13) show that the pressure perturbation p' is then given by

$$p'(\boldsymbol{x},t)=\int_{-T}^{T}\int_{V}\frac{\mathrm{D}_0^3 g(\boldsymbol{y},\tau\,|\,\boldsymbol{x},t)}{\mathrm{D}t^3}\tilde{\omega}_c\left(\tau-\frac{y_1}{U(\boldsymbol{y}_T)},\boldsymbol{y}_T\right)\mathrm{d}\boldsymbol{y}\,\mathrm{d}\tau \quad (2.14)$$

while (2.7) and (2.8) show that the corresponding transverse velocity perturbation,

$$u_\perp(\boldsymbol{x},t)\equiv u_i(\boldsymbol{x},t)\,\frac{\partial U}{\partial x_i}\Big/|\nabla U| \quad (2.15)$$

is given by

$$u_\perp=-\frac{\partial U/\partial x_i}{|\nabla U|}\int_{-T}^{T}\int_{V} g_i(\boldsymbol{y},\tau\,|\,\boldsymbol{x},t)\tilde{\omega}_c\left(\tau-\frac{y_1}{U(\boldsymbol{y}_T)},\boldsymbol{y}_T\right)\mathrm{d}\boldsymbol{y}\,\mathrm{d}\tau, \quad (2.16)$$

where

$$g_i(\boldsymbol{y}, \tau \,|\, \boldsymbol{x}, t) \equiv \frac{\mathrm{D}_0}{\mathrm{D}t}\left(\frac{\partial}{\partial x_i}\frac{\mathrm{D}_0}{\mathrm{D}t} + 2\frac{\partial U}{\partial x_i}\frac{\partial}{\partial x_1}\right) g(\boldsymbol{y}, \tau \,|\, \boldsymbol{x}, t). \tag{2.17}$$

Inserting equation (B.12) of Goldstein, Afsar & Leib (2013*b*) into this result, noting that the integral over the second term vanishes and that the relevant Poisson's equation Green's function is self-adjoint (i.e. $g_0(\boldsymbol{y}, \tau \,|\, \boldsymbol{x}, t) = g_0(\boldsymbol{x}, t \,|\, \boldsymbol{y}, \tau)$), shows that it reduces to (1.4) for two-dimensional incompressible flows with constant mean shear when the arbitrary convected quantity $\tilde{\omega}_c(\tau - y_1/U(\boldsymbol{y}_T), \boldsymbol{y}_T)$ is replaced by the renormalized convected quantity

$$\omega_c(\tau - y_1/U(\boldsymbol{y}_T)\boldsymbol{y}_T) \equiv \tilde{\omega}_c(\tau - y_1/U(\boldsymbol{y}_T), \boldsymbol{y}_T)|\boldsymbol{\nabla} U|/\rho c^2, \tag{2.18}$$

which has dimensions of vorticity (based on the rescaled velocity u_i). Equation (2.16) which, like (2.14), does not depend on the second arbitrary convected quantity $\vartheta(\tau - y_1/U, \boldsymbol{y}_T)$ is, therefore, a generalization of the Orr result (1.4). The most significant difference is that the convected quantity ω_c is no longer equal to the spanwise vorticity.

GAL show that (2.14) will apply even when solid surfaces and accompanying downstream wakes are present in the flow if $g(\boldsymbol{y}, \tau \,|\, \boldsymbol{x}, t)$ and $\vartheta(\tau - y_1/U, \boldsymbol{y}_T)$ are required to satisfy appropriate boundary conditions on these surfaces and $g(\boldsymbol{y}, \tau \,|\, \boldsymbol{x}, t)$ is required to satisfy appropriate jump conditions across the downstream wakes. The formulae (2.14) and (2.16) for the physical variables p' and $u_\perp$ can then be viewed as formal solutions to the complete non-homogeneous RDT problem (in the usual case where the solid surfaces are aligned with the constant velocity surfaces). They effectively reduce the RDT problem to the problem of finding the Rayleigh's equation Green's function that satisfies the appropriate boundary conditions on the bounding surfaces S. The solution $p'(\boldsymbol{x}, t)$ will then be independent of the second convected quantity $\vartheta(\tau - y_1/U, \boldsymbol{y}_T)$ and the acoustic field will only depend on the single convected quantity $\tilde{\omega}_c(\tau - y_1/U(\boldsymbol{y}_T), \boldsymbol{y}_T)$.

In the absence of scattering surfaces and other external sources, the unsteady flow (2.14)–(2.17) consists entirely of subsonically propagating disturbances when the mean flow is purely subsonic and, therefore, cannot radiate to the far field (Goldstein 2005, 2009). This can easily be verified in any particular case by working out the relevant far-field expansion. It is therefore appropriate to identify it with the hydrodynamic component of the motion.

3. Conservation laws for $\tilde{\omega}_c$, ϑ, transverse particle displacement and physical variables

This section summarizes the conservation laws derived in Goldstein *et al.* (2013*b*) and G79 that relate the arbitrary convected quantities $\tilde{\omega}_c(\tau - y_1/U, \boldsymbol{y}_T)$ and $\vartheta(\tau - y_1/U, \boldsymbol{y}_T)$ and a quantity, which we refer to as the transverse particle displacement, to the physical variables. The next section shows that this transverse particle displacement vanishes when $y_1 \to -\infty$ and § 5 shows how these results can be used to obtain upstream boundary conditions that relate $\tilde{\omega}_c(\tau - y_1/U, \boldsymbol{y}_T)$ and $\vartheta(\tau - y_1/U, \boldsymbol{y}_T)$ to the physical (hopefully measurable) flow variables.

The conservation laws, which are given by (3.1) and (3.2) of Goldstein *et al.* (2013*b*), can be written as

$$\frac{\partial}{\partial y_1}\left(\tilde{\omega}_c - p' - \frac{\partial N_i}{\partial y_i}\eta_\perp\right) = N_k \Gamma_{k,0} + \left(\frac{\partial N_k}{\partial y_i} - \frac{\partial N_i}{\partial y_k}\right)\Gamma_{k,i} \tag{3.1}$$

$$N_i\left(\varepsilon_{ijk}\Gamma_{k,j}+\varepsilon_{ij1}\frac{\partial\eta_\perp}{\partial y_j}\right)=0, \tag{3.2}$$

where $\tilde{\omega}_c$ is related to the rescaled vortical-like quantity ω_c by (2.18),

$$N_i\equiv\frac{c^2}{|\boldsymbol{\nabla}U|^2}\frac{\partial U}{\partial y_i}, \tag{3.3}$$

$$\Gamma_{k,0}(\boldsymbol{y},\tau)\equiv\nabla^2(u_k-u_k^{(c)})-\frac{\partial}{\partial y_k}\boldsymbol{\nabla}\cdot(\boldsymbol{u}-\boldsymbol{u}^{(c)})=\nabla^2(u_k-u_k^{(c)})+\frac{\partial}{\partial y_k}\left(c^{-2}\frac{\mathrm{D}_0p'}{\mathrm{D}\tau}\right)$$
$$-\frac{\partial}{\partial y_k}\left[(\boldsymbol{u}-\boldsymbol{u}^{(c)})\cdot c^2\boldsymbol{\nabla}\left(\frac{1}{c^2}\right)\right] \tag{3.4}$$

and

$$\Gamma_{k,i}\equiv\frac{\partial}{\partial y_i}(u_k-u_k^{(c)}),\quad\text{for } i=1,2,3 \tag{3.5}$$

are source functions and we have used (2.3) to obtain the last member of (3.4).

$$u_k^{(c)}\equiv\varepsilon_{knm}\frac{1}{c^2}\frac{\partial U}{\partial y_n}\frac{\partial\vartheta}{\partial y_m} \tag{3.6}$$

is the velocity component generated by the second convected quantity ϑ, and

$$\eta_\perp(\boldsymbol{x},t)\equiv(\partial U/\partial x_i)\lambda_i=\frac{\partial U}{\partial y_j}\left(\frac{\partial}{\partial y_j}\frac{\mathrm{D}_0\phi}{\mathrm{D}\tau}+2\frac{\partial U}{\partial y_j}\frac{\partial\phi}{\partial y_1}\right), \tag{3.7}$$

is the transverse particle displacement.

Equations (2.7) and (2.15) show that $\eta_\perp$ is related to $u_\perp$ by

$$u_\perp=\frac{1}{|\boldsymbol{\nabla}U|}\frac{\mathrm{D}_0}{\mathrm{D}\tau}\eta_\perp, \tag{3.8}$$

which justifies referring to it as the transverse particle displacement.

Equations (3.1) and (3.4)–(3.6) relate the arbitrary convected quantities $\tilde{\omega}_c(\tau-y_1/U(\boldsymbol{y}_T),\boldsymbol{y}_T)$ and $\vartheta(\tau-y_1/U(\boldsymbol{y}_T),\boldsymbol{y}_T)$ to the pressure p', density-weighted velocity $\boldsymbol{u}$ and the transverse particle displacement $\eta_\perp$, while (3.2) and (3.4)–(3.6) relate the arbitrary convected quantity $\vartheta(\tau-y_1/U(\boldsymbol{y}_T),\boldsymbol{y}_T)$ to the pressure p', density-weighted velocity $\boldsymbol{u}$ and the transverse particle displacement $\eta_\perp$.

The tensor $(\partial N_k/\partial y_i-\partial N_i/\partial y_k)$ is equal to zero and $u_k^{(c)}$ drops out of the first term on the right-hand side of (3.4) for planar base flows, where c^2 and U depend on a single Cartesian coordinate (say y_2) and (3.1) then becomes

$$\frac{\partial}{\partial y_1}\left(\tilde{\omega}_c-p'-\frac{\mathrm{d}N_2}{\mathrm{d}y_2}\eta_\perp\right)=N_2\left[\boldsymbol{\nabla}\cdot[c^{-2}\boldsymbol{\nabla}(c^2u_2)]+\frac{\partial}{\partial y_2}\left(c^{-2}\frac{\mathrm{D}_0p'}{\mathrm{D}\tau}\right)\right], \tag{3.9}$$

which is independent of $u_i^{(c)}$ and, therefore, of the second convected quantity ϑ. But the divergence $\partial N_i/\partial y_i$ is equal to zero for the constant shear-constant c^2 parallel mean flow (1.1), since N_i is a constant in that case, and it follows from (2.18) that (3.9) then reduces to Möhring's (1976) result

$$\frac{\partial}{\partial y_1}\left(\rho\omega_c-\frac{\gamma p'}{c^2}\right)=\boldsymbol{\nabla}\cdot[c^{-2}\boldsymbol{\nabla}(c^2u_2)]+\frac{\partial}{\partial y_2}\left(c^{-2}\frac{\mathrm{D}_0p'}{\mathrm{D}\tau}\right) \tag{3.10}$$

and to Orr's equation (1.3) when the flow is incompressible and two-dimensional.

The particle displacement $\eta_\perp$ which appears in equations (3.1) and (3.2) is not actually a physical variable in the usual sense, and requires further clarification, which is provided in the next section. However, our interest here is in obtaining a set of upstream boundary conditions that relate $\tilde{\omega}_c$ and ϑ to the physically measurable variables at upstream infinity, which can be obtained by taking the limit as $y_1 \to -\infty$ of these equations. This greatly simplifies the formulae and, as will be shown below, even allows us to obtain an explicit formula for $\tilde{\omega}_c$.

4. Particle displacement and causality

As indicated in the paragraphs above and below equations (2.11) and (2.12), our interest is in time-stationary solutions which are assumed to exist for the physical variables p' and $u_\perp$. It is therefore appropriate to work with the temporal Fourier transforms

$$\bar{p}'(\boldsymbol{x}:\omega) \equiv \lim_{T\to\infty} \frac{1}{2\pi} \int_{-T}^{T} \mathrm{e}^{\mathrm{i}\omega t} p'(\boldsymbol{x}, t)\, \mathrm{d}t, \quad \bar{u}_\perp(\boldsymbol{x}:\omega) \equiv \lim_{T\to\infty} \frac{1}{2\pi} \int_{-T}^{T} \mathrm{e}^{\mathrm{i}\omega t} u_\perp(\boldsymbol{x}, t)\, \mathrm{d}t, \tag{4.1a,b}$$

where the integrals are to be interpreted in a stochastic sense and the limits are to be taken after the statistical quantities are calculated (Wiener 1938). (Laplace transforms would not be appropriate here.) However, the formula (2.13) for the potential ϕ is still only formal in that the integrand on the right-hand side has a non-integrable singularity at $\boldsymbol{y} = \boldsymbol{x}$. But the corresponding integrands in (2.14) and (2.16) for the physical variables p' and $u_\perp$ remain finite, and these quantities are therefore (stochastically) well defined. In fact, GAL, G78 and G79 show that they are given by

$$\bar{p}'(\boldsymbol{x}:\omega) = (2\pi)^2 \int_{A_T} \mathrm{e}^{\mathrm{i}\omega x_1/U(\boldsymbol{y}_T)} \bar{G}_0(\boldsymbol{y}_T \,|\, \boldsymbol{x}_T : \omega, \omega/U(\boldsymbol{y}_T)) \bar{\Omega}_c(\boldsymbol{y}_T : \omega)\, \mathrm{d}\boldsymbol{y}_T, \tag{4.2}$$

and

$$\bar{u}_\perp(\boldsymbol{x}:\omega) = -(2\pi)^2 \frac{\partial U}{\partial x_i} \frac{1}{|\nabla U|} \int_{A_T} \mathrm{e}^{\mathrm{i}\omega x_1/U(\boldsymbol{y}_T)} \bar{G}_i(\boldsymbol{y}_T \,|\, \boldsymbol{x}_T : \omega, \omega/U(\boldsymbol{y}_T)) \bar{\Omega}_c(\boldsymbol{y}_T : \omega)\, \mathrm{d}\boldsymbol{y}_T, \tag{4.3}$$

respectively, where $\boldsymbol{y}_T$ is defined below (2.3), A_T denotes the cross-sectional area such that $\int_{A_T} \int_{-\infty}^{\infty} \cdot\, \mathrm{d}\boldsymbol{y}_T\, \mathrm{d}y_1 = \int_V \cdot\, \mathrm{d}\boldsymbol{y}$, $\bar{\Omega}_c(\boldsymbol{x}:\omega)$ is defined as the limit $T \to \infty$ of

$$\bar{\Omega}_c(\boldsymbol{y}_T : \omega, T) \equiv \frac{1}{2\pi} \int_{-T}^{T} \mathrm{e}^{\mathrm{i}\omega z} \tilde{\omega}_c(z, \boldsymbol{y}_T)\, \mathrm{d}z, \tag{4.4}$$

$$\bar{G}_0(\boldsymbol{y}_T \,|\, \boldsymbol{x}_T : \omega, \omega/U(\boldsymbol{y}_T)) \equiv \lim_{k_1 \to \omega/U(\boldsymbol{y}_T)} \bar{G}_0(\boldsymbol{y}_\perp \,|\, \boldsymbol{x}_\perp : \omega, k_1), \tag{4.5}$$

where

$$\bar{G}_0(\boldsymbol{y}_\perp \,|\, \boldsymbol{x}_\perp : \omega, k_1) \equiv \frac{[\mathrm{i}k_1 U(\boldsymbol{x}_T) - \mathrm{i}\omega]^3}{(2\pi)^2} \times \int_{-\infty}^{\infty} \int_{-\infty}^{\infty} \mathrm{e}^{\mathrm{i}[k_1(y_1 - x_1) + \omega(t-\tau)]} g(\boldsymbol{y}, \tau \,|\, \boldsymbol{x}, t)\, \mathrm{d}(y_1 - x_1)\, \mathrm{d}(t - \tau) \tag{4.6}$$

satisfies the reduced inhomogeneous Rayleigh's equation

$$L_R\bar{G}_0 \equiv \frac{1}{(2\pi)^2}\delta(\boldsymbol{x}_T - \boldsymbol{y}_T), \tag{4.7}$$

with L_R being the reduced Rayleigh operator

$$L_R \equiv \nabla_T \cdot \left\{ \frac{c^2\nabla_T}{[\omega - U(\boldsymbol{y}_T)k_1]^2} \right\} + 1 - \frac{c^2k_1^2}{[\omega - U(\boldsymbol{y}_T)k_1]^2} \tag{4.8}$$

written in terms of the Laplacian ∇_T with respect to the transverse coordinate $\boldsymbol{y}_T$. Appendix A shows that $\bar{G}_0(\boldsymbol{y}_T\,|\,\boldsymbol{x}_T : \omega, \omega/U(\boldsymbol{y}_T))$ remains finite and is continuous at $\boldsymbol{y}_T = \boldsymbol{x}_T$ for two-dimensional mean flows, and a similar analysis would show that this is true in general, but the notation becomes very tedious in that case. Appendix A also shows that

$$\bar{G}_i(\boldsymbol{y}_T\,|\,\boldsymbol{x}_T : \omega, k_1) \equiv \frac{1}{[\mathrm{i}k_1U(\boldsymbol{x}_T) - \mathrm{i}\omega]}\frac{\partial}{\partial x_i}\bar{G}_0(\boldsymbol{y}_T\,|\,\boldsymbol{x}_T : \omega, k_1), \quad i = 1, 2, 3 \tag{4.9}$$

remains finite and continuous at $\boldsymbol{y}_T = \boldsymbol{x}_T$ for two-dimensional mean flows. It therefore follows from (4.3), the first line of (B 4), (B 6) and inversion of the Fourier transform (4.1) that

$$\bar{u}_\perp(\boldsymbol{x} : \omega) \to \frac{\mathrm{e}^{\mathrm{i}\omega x_1/U(x_2)}}{x_1^2}\bar{\mathcal{U}}_\perp(\boldsymbol{x}_T, \omega), \quad \text{as } x_1 \to -\infty \tag{4.10}$$

and

$$u_\perp(\boldsymbol{x}, t) \to \frac{1}{x_1^2}\mathcal{U}_\perp(t - x_1/U(x_2), \boldsymbol{x}_T), \quad \text{as } x_1 \to -\infty, \tag{4.11}$$

where the purely convected quantity $\mathcal{U}_\perp(t - x_1/U(x_2), \boldsymbol{x}_T)$ is a function of the indicated arguments and $\bar{\mathcal{U}}_\perp(\boldsymbol{x}_T, \omega)$ is the Fourier transform of that quantity. The comment below (4.8) suggests that these results, which generalize the behaviour discussed in the introduction, are expected to apply to much more general transversely sheared mean flows (such as those described below) even though they were derived for two-dimensional base flows.

The Fourier transform

$$\bar{\eta}_\perp(\boldsymbol{x}, \omega) \equiv \lim_{T\to\infty}\frac{1}{2\pi}\int_{-T}^{T}\mathrm{e}^{\mathrm{i}\omega t}\eta_\perp(\boldsymbol{x}, t)\,\mathrm{d}t \tag{4.12}$$

of the transverse particle displacement (3.7), which formally satisfies

$$\frac{\partial\bar{\eta}_\perp(\boldsymbol{x}, \omega)}{\partial x_1} = -(2\pi)^2\frac{\partial U}{\partial x_i}\int_{A_T}\mathrm{e}^{\mathrm{i}\omega x_1/U(\boldsymbol{y}_T)}\frac{\bar{G}_i(\boldsymbol{y}_T\,|\,\boldsymbol{x}_T : \omega, \omega/U(\boldsymbol{y}_T))}{U(\boldsymbol{x}_T) - U(\boldsymbol{y}_T)}\bar{\Omega}_c(\boldsymbol{y}_T : \omega)\,\mathrm{d}\boldsymbol{y}_T, \tag{4.13}$$

will become unbounded at $\boldsymbol{y} = \boldsymbol{x}$ since, as shown in appendix A for the two-dimensional case, $\bar{G}_i(\boldsymbol{y}_T\,|\,\boldsymbol{x} : \omega, \omega/U(\boldsymbol{y}_T))$ will usually not vanish when $\boldsymbol{y}_T = \boldsymbol{x}_T$. It can be made finite in a number of ways. But there is only one possibility if causality is also imposed. This amounts to assuming that the time-stationary solutions will exist even when $\eta_\perp(\boldsymbol{x}, t)$ is assumed to be identically zero in the distant past. This can be implemented by using the Briggs (1964)–Bers (1975) procedure, which amounts to letting ω have a small positive imaginary part, say ε, and taking the

limit as $\varepsilon \to 0$ of the resulting formula. It is not possible to do this directly in the present case, but (4.13) can represented as the limit of a sequence and this procedure can be used to impose causality on each term of that sequence. (Details are given in appendix C.) It could, however, be argued that $\eta_\perp$ need not be causal because it is not actually a physical variable, but the conservation laws (3.1)–(3.2) and, more importantly, the upstream boundary conditions would then also be non-causal. Our primary interest is in the upstream behaviour of $\eta_\perp$, which will be used to derive the upstream boundary conditions referred to in the introduction. The analysis in appendix C shows that

$$\frac{\partial \bar{\eta}_\perp(\boldsymbol{x}, \omega)}{\partial x_1} \to 0, \quad \text{as } x_1 \to -\infty \tag{4.14}$$

when causality is imposed, which implies that

$$\frac{\partial \eta_\perp(\boldsymbol{x}, t)}{\partial x_1} \to 0, \quad \text{as } x_1 \to -\infty \tag{4.15}$$

in this case. Different results would be possible if causality were not imposed.

5. Upstream boundary conditions and relation of $\tilde{\omega}_c$, ϑ to the physical variables

It is useful, although not essential, to first split the dependent variables into a hydrodynamic component, which does not directly produce any sound at subsonic Mach numbers, and a non-hydrodynamic component, which accounts for the remaining – including the acoustic – components of the motion, before attempting to derive the relevant boundary conditions. We can then think of the former component as being an upstream 'input' that generates a downstream 'response' when it interacts with streamwise changes in the boundary conditions.

As is well known, it is impossible to unambiguously decompose the unsteady motion on a transversely sheared mean flow into acoustic and hydrodynamic components. We can, however, require that the hydrodynamic component not radiate any sound at subsonic Mach numbers, with all the acoustic radiation being accounted for by the remaining non-hydrodynamic component. Then, in order to identify the input disturbance with the hydrodynamic component of the motion, we divide the Rayleigh equation Green's function $g(\boldsymbol{y}, \tau \,|\, \boldsymbol{x}, t)$ that appears in the time-dependent solution (2.13)–(2.16) into two components, say

$$g(\boldsymbol{y}, \tau \,|\, \boldsymbol{x}, t) = g^{(H)}(\boldsymbol{y}, \tau \,|\, \boldsymbol{x}, t) + g^{(s)}(\boldsymbol{y}, \tau \,|\, \boldsymbol{x}, t), \tag{5.1}$$

where $g^{(H)}(\boldsymbol{y}, \tau \,|\, \boldsymbol{x}, t)$ denotes a particular solution of (2.12) which is defined on all space when the bounding surfaces S are all at infinity or, more generally, satisfies appropriate boundary conditions (given in Goldstein *et al.* 2013*a*,*b*) on a constant mean velocity surface that extends from minus to plus infinity in the streamwise direction. The corresponding solution, which is given by (2.14) and (2.16) with $g(\boldsymbol{y}, \tau \,|\, \boldsymbol{x}, t)$ replaced by $g^{(H)}(\boldsymbol{y}, \tau \,|\, \boldsymbol{x}, t)$, does not produce any acoustic radiation and can, therefore, be identified with the hydrodynamic component of the unsteady motion. The corresponding 'scattered solution', $g^{(s)}(\boldsymbol{y}, \tau \,|\, \boldsymbol{x}, t)$, satisfies the homogeneous Rayleigh's equation along with appropriate inhomogeneous boundary and jump conditions on the streamwise discontinuous surfaces S and, therefore, accounts for all of the acoustic components of the motion.

We now obtain the relevant upstream boundary conditions for the convected quantities $\tilde{\omega}_c$ and ϑ by taking the upstream limit of (3.1) and (3.2), but with $g(\boldsymbol{y}, \tau \,|\, \boldsymbol{x}, t)$ replaced by $g^{(H)}(\boldsymbol{y}, \tau \,|\, \boldsymbol{x}, t)$. This is most easily done by using the frequency representation discussed in § 3. The reduced Rayleigh equation Green's function $\bar{G}_0(\boldsymbol{y}_T \,|\, \boldsymbol{x} : \omega, k_1)$ that appears in the frequency domain solutions (4.2), (4.3) and (4.13) then has the decomposition

$$\bar{G}_0(\boldsymbol{y}_T \,|\, \boldsymbol{x} : \omega, k_1) = \bar{G}^{(H)}(\boldsymbol{y}_T \,|\, \boldsymbol{x} : \omega, k_1) + \bar{G}^{(s)}(\boldsymbol{y}_T \,|\, \boldsymbol{x} : \omega, k_1), \tag{5.2}$$

where $\bar{G}^{(H)}(\boldsymbol{y}_T \,|\, \boldsymbol{x} : \omega, k_1)$ is either defined on all space when the bounding surfaces S are all at infinity or satisfies

$$\frac{\hat{n}_j}{[\omega - k_1 U(\boldsymbol{y}_T)]^2} \frac{\partial}{\partial y_j} \bar{G}^{(H)}(\boldsymbol{y}_T \,|\, \boldsymbol{x} : \omega, k_1) = 0, \quad \text{for } \boldsymbol{y}_T \in C_T, \tag{5.3}$$

(where C_T denotes the bounding curve/curves that generate the doubly infinite surface/surfaces S) when they are not. The streamwise-homogeneous Green's functions $g^{(H)}(\boldsymbol{y}, \tau \,|\, \boldsymbol{x}, t)$ and $\bar{G}^{(H)}(\boldsymbol{y}_T \,|\, \boldsymbol{x} : \omega, k_1)$ will then depend on y_1 and x_1 only in the combination $x_1 - y_1$ and we, therefore, write

$$\bar{G}^{(H)}(\boldsymbol{y}_T \,|\, \boldsymbol{x} : \omega, k_1) = \bar{G}^{(H)}(\boldsymbol{y}_T \,|\, \boldsymbol{x}_T : \omega, k_1). \tag{5.4}$$

The convected quantity $\tilde{\omega}_c$ is determined by (3.1) and (3.2), whose Fourier transforms are given by

$$\begin{aligned} &\frac{\partial}{\partial y_1}[\mathrm{e}^{\mathrm{i}\omega y_1/U(y_T)} \bar{\Omega}_c(\boldsymbol{y}_T : \omega) - \bar{p}'(\boldsymbol{y} : \omega)] - \frac{\mathrm{d}N_i}{\mathrm{d}y_i} \frac{\partial \bar{\eta}_\perp^{(H)}(\boldsymbol{y} : \omega)}{\partial y_1} \\ &\quad = \mathrm{e}^{\mathrm{i}\omega y_1/U(y_T)} \left[N_k \bar{\Gamma}_{k,0}(\boldsymbol{y} : \omega) + \left(\frac{\partial N_k}{\partial y_i} - \frac{\partial N_i}{\partial y_k} \right) \bar{\Gamma}_{k,i}(\boldsymbol{y} : \omega) \right] \end{aligned} \tag{5.5}$$

and

$$N_i \left(\varepsilon_{ijk} \bar{\Gamma}_{k,j} + \varepsilon_{ij1} \frac{\partial \bar{\eta}_\perp^{(H)}}{\partial y_j} \right) = 0, \tag{5.6}$$

where $\bar{\eta}_\perp^{(H)}(\boldsymbol{y} : \omega)$ is given by (4.13) with $\bar{G}_i(\boldsymbol{y}_T \,|\, \boldsymbol{x} : \omega, k_1)$ replaced by $\bar{G}_i^{(H)}(\boldsymbol{y}_T \,|\, \boldsymbol{x} : \omega, k_1)$

$$\bar{\Omega}_c(\boldsymbol{y}_T : \omega) \equiv \lim_{T \to \infty} \bar{\Omega}_c(\boldsymbol{y}_T : \omega, T) \tag{5.7}$$

and $\bar{\Gamma}_{k,i}(\boldsymbol{y} : \omega) \equiv \lim_{T \to \infty} \bar{\Gamma}_{k,i}(\boldsymbol{y} : \omega, T)$ for $k = 0, 1, 2, 3$ with

$$\bar{\Gamma}_{k,i}(\boldsymbol{y} : \omega, T) \equiv \frac{1}{2\pi} \int_{-T}^{T} \mathrm{e}^{\mathrm{i}\omega[\tau - y_1/U(y_T)]} \Gamma_{k,i}(\boldsymbol{y}, \tau) \, \mathrm{d}\tau, \tag{5.8}$$

where $\Gamma_{k,i}$, $i = 0, 1, 2, 3$, are defined by (3.4) and (3.5).

Then, since we have shown that the Fourier transform $\bar{\eta}_\perp^{(H)}(\boldsymbol{y} : \omega)$ of the transverse particle displacement $\eta_\perp^{(H)}$ vanishes as $y_1 \to -\infty$, and an argument similar to that used to obtain (B 6) shows that $\bar{p}'(\boldsymbol{y} : \omega)$ should vanish like y_1^{-2} as $y_1 \to -\infty$, (5.5) and (5.6) imply that

$$\bar{\Omega}_c(\boldsymbol{y}_T : \omega, T) \to \frac{1}{\mathrm{i}\omega} U(\boldsymbol{y}_T) \left[N_k \bar{\Gamma}_{k,0}^{\infty}(\boldsymbol{y} : \omega) + \left(\frac{\partial N_k}{\partial y_i} - \frac{\partial N_i}{\partial y_k} \right) \bar{\Gamma}_{k,i}^{\infty} \right], \quad \text{as } y_1 \to -\infty \tag{5.9}$$

and

$$N_i \varepsilon_{ijk} \bar{\Gamma}^{\infty}_{k,j} \to 0, \tag{5.10}$$

where

$$\bar{\Gamma}^{\infty}_{k,i}(\boldsymbol{y} : \omega, T) \equiv \lim_{y_1 \to -\infty} \bar{\Gamma}_{k,i}(\boldsymbol{y} : \omega, T). \tag{5.11}$$

These results provide the desired relations between the convected quantities $\tilde{\omega}_c(\tau - y_1/U(\boldsymbol{y}_T), \boldsymbol{y}_T)$, $\vartheta(\tau - y_1/U(\boldsymbol{y}_T), \boldsymbol{y}_T)$ and the upstream limit $\bar{\Gamma}^{\infty}_{k,i}(\boldsymbol{y} : \omega)$, for $i = 0, 1, 2, 3$ of the physically measurable variables that enter through $\Gamma_{k,i}(\boldsymbol{y}, \tau)$ in an arbitrary transversely sheared mean flow.

But the focus in the remainder of the paper will be on the two-dimensional mean flows for which $\partial N_k/\partial y_i - \partial N_i/\partial y_k = 0$ and (5.9) becomes

$$\hat{\Omega}_c(y_2 : \omega, k_3, T) = \frac{1}{\mathrm{i}\omega} U(y_2) N_2 \hat{\Gamma}_{\infty}, \tag{5.12}$$

where

$$\begin{aligned} \hat{\Omega}_c(y_2; \omega, k_3, T) &\equiv \frac{1}{2\pi} \int_{-T}^{T} \mathrm{e}^{-\mathrm{i}y_3 k_3} \bar{\Omega}_c(\boldsymbol{y}_T : \omega, T)\, \mathrm{d}y_3 \\ &= \frac{1}{(2\pi)^2} \int_{-T}^{T} \mathrm{e}^{-\mathrm{i}y_3 k_3} \int_{-T}^{T} \mathrm{e}^{\mathrm{i}\omega\xi} \tilde{\omega}_c(\xi, \boldsymbol{y}_T)\, \mathrm{d}\xi\, \mathrm{d}y_3 \end{aligned} \tag{5.13}$$

is the double Fourier transform of the convected quantity $\tilde{\omega}_c(\xi, \boldsymbol{y}_T)$ and

$$\begin{aligned} \hat{\Gamma}_{\infty}(y_2; \omega, k_3, T) &= \frac{1}{2\pi} \int_{-\infty}^{\infty} \mathrm{e}^{-\mathrm{i}y_3 k_3} \bar{\Gamma}^{\infty}_{2,0}(\boldsymbol{y}_T : \omega, T)\, \mathrm{d}y_3 \\ &= \frac{1}{(2\pi)^2} \lim_{y_1 \to -\infty} \int_{-\infty}^{\infty} \mathrm{e}^{-\mathrm{i}y_3 k_3} \int_{-T}^{T} \mathrm{e}^{\mathrm{i}\omega[\tau - y_1/U(\boldsymbol{y}_T)]} \Gamma_{2,0}(\boldsymbol{y}, \tau)\, \mathrm{d}\tau\, \mathrm{d}y_3 \end{aligned} \tag{5.14}$$

is the upstream limit of the double Fourier transform of the physically measurable vorticity derivative $\Gamma_{2,0}$ given by (3.4).

But (3.4) and (3.6) imply that

$$\Gamma_{2,0}(\boldsymbol{y}, \tau) = \nabla^2 u_2 - \frac{\partial}{\partial y_2} \boldsymbol{\nabla} \cdot \boldsymbol{u} = \boldsymbol{\nabla} \cdot [c^{-2} \boldsymbol{\nabla}(c^2 u_2)] + \frac{\partial}{\partial y_2} \left(c^{-2} \frac{\mathrm{D}_0 p'}{\mathrm{D}\tau} \right) \tag{5.15}$$

for two-dimensional mean flows and, therefore that $\Gamma_{2,0}(\boldsymbol{y}, \tau)$ and, consequently, $\hat{\Gamma}_{\infty}(y_2; \omega, k_3, T)$ only depend on the physical variables u_2 and p' for these mean flows. Equation (5.12) therefore provides the desired upstream boundary condition that relates the Fourier transform of the unknown convected quantity $\tilde{\omega}_c(\tau - y_1/U(\boldsymbol{y}_T), \boldsymbol{y}_T)$ to the physically measurable quantity (5.15) in this case.

But we can go even further than this, since an argument similar to that given at the end of appendix B can be used to show that p' should vanish like $1/y_1^2$ as $y_1 \to -\infty$, and $\lim_{y_1 \to \infty} \Gamma_{2,0}$ is, therefore, given by $\boldsymbol{\nabla} \cdot [c^{-2} \boldsymbol{\nabla}(c^2 u_2)]$. Inserting (4.11) into this result, noting that $u_{\perp}(\boldsymbol{x}, t) = u_2(\boldsymbol{x}, t)$ in this case, shows that

$$\boldsymbol{\nabla} \cdot [c^{-2} \boldsymbol{\nabla}(c^2 u_2)] \to \frac{\partial^2 u_2}{\partial y_2^2} \to \left[\frac{\partial U(y_2)/\partial y_2}{U^2(y_2)} \right]^2 \frac{\partial^2}{\partial \tau^2} \mathcal{U}_2(\tau - y_1/U(y_2), \boldsymbol{y}_T), \quad y_1 \to -\infty. \tag{5.16}$$

Inserting this into (5.8) and (5.11), and integrating the result by parts shows that

$$\bar{\Gamma}^{\infty}_{2,0}(\boldsymbol{y}:\omega,T)=\bar{\Gamma}^{\infty}_{2,0}(\boldsymbol{y}_T:\omega,T)=\frac{1}{2\pi}\int_{-T}^{T}\mathrm{e}^{\mathrm{i}\omega[\tau-y_1/U(\boldsymbol{y}_T)]}\Gamma_\infty(\boldsymbol{y},\tau)\,\mathrm{d}\tau, \tag{5.17}$$

where

$$\Gamma_\infty(\boldsymbol{y},\tau)\equiv\left[\frac{\partial U(y_2)/\partial y_2}{U^2(y_2)}\right]^2\frac{\partial^2}{\partial\tau^2}\mathcal{U}_\perp(\tau-y_1/U(\boldsymbol{y}_T),\boldsymbol{y}_T)=\Gamma_\infty(\tau-y_1/U(\boldsymbol{y}_T),\boldsymbol{y}_T). \tag{5.18}$$

6. Relation between the $\tilde{\omega}_c$ spectra and measurable turbulence correlations

But only statistical quantities, such as

$$\overbrace{\hat{\Gamma}_\infty(\boldsymbol{y},\tau)\hat{\Gamma}_\infty(\tilde{y},\tau+\tilde{\tau})}\equiv\lim_{T\to\infty}\frac{1}{2T}\int_{-T}^{T}\hat{\Gamma}_\infty(\boldsymbol{y},\tau)\hat{\Gamma}_\infty(\tilde{y},\tau+\tilde{\tau})\,\mathrm{d}\tau, \tag{6.1}$$

where $\hat{\Gamma}_\infty$ is defined by (5.15) and (5.14), are of interest for the time-stationary turbulent flows that are the main focus of RDT. For simplicity, we only consider mean flows that are uniform in the y_3-direction and suppose that the turbulence is statistically homogeneous in the spanwise direction. Then the space–time average

$$\begin{aligned}&\langle\Gamma_\infty(\boldsymbol{y},\tau)\Gamma_\infty(y_1,\tilde{y}_2,y_3+\eta_3,\tau+\tilde{\tau})\rangle\\&\quad\equiv\lim_{T\to\infty}\frac{1}{2T}\int_{-T}^{T}\int_{-\infty}^{\infty}\Gamma_\infty(\boldsymbol{y}_T,\tau-y_1/U(y_2))\Gamma_\infty(\tilde{y}_2,y_3+\eta_3,\tau-\tilde{y}_1/U(\tilde{y}_2)+\tilde{\tau})\,\mathrm{d}\tau\,\mathrm{d}y_3\\&\quad=\lim_{T\to\infty}\frac{1}{2T}\int_{-T}^{T}\int_{-\infty}^{\infty}\Gamma_\infty(\boldsymbol{y}_T,\tau)\Gamma_\infty(\tilde{y}_2,y_3+\eta_3,\tau+\tilde{\tau}-[y_1/U(\tilde{y}_2)-y_1/U(y_2)])\,\mathrm{d}\tau\,\mathrm{d}y_3\end{aligned} \tag{6.2}$$

will exist and be independent of τ, y_3 and it follows from the convolution theorem that

$$\begin{aligned}&\frac{1}{(2\pi)^2}\int_{-\infty}^{\infty}\int_{-\infty}^{\infty}\exp\{\mathrm{i}[\omega(\tilde{\tau}-[\tilde{y}_1/U(\tilde{y}_2)-y_1/U(y_2)])-k_3\eta_3]\}\\&\qquad\times\langle\Gamma_\infty(\boldsymbol{y},\tau)\Gamma_\infty(\tilde{y}_1,\tilde{y}_2,y_3+\eta_3,\tau+\tilde{\tau})\rangle\,\mathrm{d}\tilde{\tau}\,\mathrm{d}\eta_3\\&\quad=(2\pi)^2\lim_{T\to\infty}\frac{\hat{\Gamma}_\infty(y_2;\omega,k_3,T)[\hat{\Gamma}_\infty(\tilde{y}_2;\omega,k_3,T)]^*}{2T},\end{aligned} \tag{6.3}$$

where $\hat{\Gamma}_\infty(y_2;\omega,k_3,T)$ is given by (5.14) and the asterisk denotes the complex conjugate.

It, therefore, follows from (5.12) and (6.3) that

$$\begin{aligned}&S(y_2,\tilde{y}_2:k_3,\omega)\\&\quad\equiv(2\pi)^3\lim_{T\to\infty}\frac{\hat{\Omega}_c(y_2:\omega,k_3;T)\hat{\Omega}_c^*(\tilde{y}_2:\omega,k_3;T)}{2T}\\&\quad=\frac{1}{2\pi}\int_{-\infty}^{\infty}\int_{-\infty}^{\infty}\mathrm{e}^{\mathrm{i}(\omega\tilde{\tau}-k_3\eta_3)}\langle\tilde{\omega}_c(t,\boldsymbol{y}_T)\tilde{\omega}_c(t+\tilde{\tau},\tilde{y}_2,y_3+\eta_3)\rangle\,\mathrm{d}\tilde{\tau}\,\mathrm{d}\eta_3\\&\quad=\frac{U(y_2)U(\tilde{y}_2)N_2\tilde{N}_2}{2\pi\omega^2}\int_{-\infty}^{\infty}\int_{-\infty}^{\infty}\mathrm{e}^{\{\mathrm{i}[\omega(\tilde{\tau}-[\tilde{y}_1/U(\tilde{y}_2)-y_1/U(y_2)])-k_3\eta_3]\}}\\&\qquad\times\langle\Gamma_\infty(y,t)\Gamma_\infty(\tilde{y}_1,\tilde{y}_2,y_3+\eta_3,t+\tilde{\tau})\rangle\,\mathrm{d}\tilde{\tau}\,\mathrm{d}\eta_3,\end{aligned} \tag{6.4}$$

where $\hat{\Omega}_c(y_2:\omega,k_3,T)$ is given by (5.13).

6.1. *Source model*

Since the problem is linear, it follows from (4.3) and (5.13) that the complete solution to any problem where the surface extends continuously from $-\infty < x_3 < \infty$, say for the Fourier-transformed transverse velocity fluctuation $\bar{u}_\perp(x_1, x_2; k_3, \omega)$, must be of the form

$$\bar{u}_\perp(x_1, x_2; \omega, k_3) = \int_{l_T} \mathcal{R}(y_2 \,|\, x_1, x_2; \omega, k_3)\hat{\Omega}(y_2 : \omega, k_3)\,\mathrm{d}y_2, \tag{6.5}$$

which means that knowledge of $\hat{\Omega}(y_2 : \omega, k_3)$ is all that is actually needed for the two-dimensional mean flow solutions being considered here. A similar formula would, of course, also hold for the Fourier-transformed pressure fluctuation $\hat{p}'(x_1, x_2; k_3, \omega)$.

The spectrum, $S(y_2, \tilde{y}_2 : k_3, \omega)$ of the convected quantity $\tilde{\omega}_c$, which is related to the cross-correlation $\langle \Gamma_\infty(\boldsymbol{y}, t)\Gamma_\infty(\tilde{y}_1, \tilde{y}_2, y_3 + \eta_3, t + \tilde{\tau})\rangle$ of the upstream vorticity fluctuation by (6.4) needs to be specified before formulae for the acoustic spectrum such as the one derived in GAL can actually be used. While (5.18) and (5.16) show that

$$\Gamma_\infty(\boldsymbol{y}, \tau) = \lim_{y_1 \to -\infty} \boldsymbol{\nabla} \cdot [c^{-2}\boldsymbol{\nabla}(c^2 u_2)] \tag{6.6}$$

and therefore $\langle \Gamma_\infty(\boldsymbol{y},t)\Gamma_\infty(\tilde{y}_1, \tilde{y}_2, y_3 + \eta_3, t + \tilde{\tau})\rangle$ corresponds to a physically measurable correlation, we are unaware of any measurements of this quantity that have actually been carried out. But the transverse velocity correlation $\langle v_2'(t, \boldsymbol{y})v_2'(t + \tilde{\tau}, \tilde{y})\rangle$, which has been extensively measured, can be well represented by the exponential form

$$\begin{aligned} &A(y_2, \tilde{y}_2)\rho(y_2)\rho(\tilde{y}_2)\left\{1 + a_1(\tilde{\tau} - [\tilde{y}_1/U(\tilde{y}_2) - y_1/U(y_2)])\frac{\partial}{\partial \tilde{\tau}}\right\} \\ &\quad \times \exp -\sqrt{[f(\eta_2/l_2)]^2 + \{\tilde{\tau} - [\tilde{y}_1/U(\tilde{y}_2) - y_1/U(y_2)]\}^2/\tau_0^2 + (\eta_3/l_3)^2}, \end{aligned} \tag{6.7}$$

where the derivative term accounts for the negative tail of the correlation and the amplitude $A(y_2, \tilde{y}_2)$ is expected to vanish as $y_2, \tilde{y}_2 \to 0, \infty$. We therefore initially suppose that $\langle \mathcal{U}_\perp(t - y_1/U(y_2), \boldsymbol{y}_T)\mathcal{U}_\perp(t + \tilde{\tau} - \tilde{y}_1/U(\tilde{y}_2), \tilde{y}_2, y_3 + \eta)\rangle = \lim_{y_1 \to -\infty} y_1^4 \langle u_\perp(y_1, \boldsymbol{y}_T, t)u_\perp(y_1, \tilde{\boldsymbol{y}}_T, t + \tilde{\tau})\rangle = \lim_{y_1 \to -\infty} y_1^4 \langle \rho v_\perp'(y_1, \boldsymbol{y}_T, t)\rho v_\perp'(y_1, \tilde{\boldsymbol{y}}_T, t + \tilde{\tau})\rangle$ can be modelled by

$$\begin{aligned} &\langle \mathcal{U}_\perp(t - y_1/U(y_2), \boldsymbol{y}_T)\mathcal{U}_\perp(t + \tilde{\tau} - \tilde{y}_1/U(\tilde{y}_2), \tilde{y}_2, y_3 + \eta_3)\rangle \\ &\quad = A(y_2, \tilde{y}_2)l_2^4\rho(y_2)\rho(\tilde{y}_2)\left\{1 + a_1(\tilde{\tau} - [\tilde{y}_1/U(\tilde{y}_2) - y_1/U(y_2)])\frac{\partial}{\partial \tilde{\tau}}\right\} \\ &\qquad \times \exp -\sqrt{[f(\eta_2/l_2)]^2 + \{\tilde{\tau} - [\tilde{y}_1/U(\tilde{y}_2) - y_1/U(y_2)]\}^2/\tau_0^2 + (\eta_3/l_3)^2}, \end{aligned} \tag{6.8}$$

which as shown by (5.18) is related to $\langle \Gamma_\infty(\boldsymbol{y}, t)\Gamma_\infty(\tilde{y}_1, \tilde{y}_2, y_3 + \eta_3, t + \tilde{\tau})\rangle$ by

$$\begin{aligned} \langle \Gamma_\infty(\boldsymbol{y}, t)\Gamma_\infty(\tilde{y}_1, \tilde{y}_2, y_3 + \eta_3, t + \tilde{\tau})\rangle &= \left[\frac{(\mathrm{d}U/\mathrm{d}y_2)(\mathrm{d}U/\mathrm{d}\tilde{y}_2)}{U^2(\tilde{y}_2)U^2(y_2)}\right]^2 \frac{\partial^4}{\partial \tau^4} \\ &\quad \times \langle \mathcal{U}_\perp(t - y_1/U(y_2), \boldsymbol{y}_T)\mathcal{U}_\perp(t + \tilde{\tau} - \tilde{y}_1/U(\tilde{y}_2), \tilde{y}_2, y_3 + \eta)\rangle. \end{aligned} \tag{6.9}$$

Equation (40) of Leib & Goldstein (2011) can be used to show that the spectrum (6.3) of this quantity is given by the following Hankel transform

$$\int_{-\infty}^{\infty}\int_{-\infty}^{\infty} \mathrm{e}^{\mathrm{i}[\omega(\tilde{\tau}-[\tilde{y}_1/U(\tilde{y}_2)-y_1/U(y_2)])-k_3\eta_3]}\langle \Gamma_\infty(\boldsymbol{y},t)\Gamma_\infty(\tilde{y}_1,\tilde{y}_2,y_3+\eta_3,t+\tilde{\tau})\rangle \,\mathrm{d}\tilde{\tau}\,\mathrm{d}\eta_3$$
$$= 2\pi\tau_0 l_3 l_2^4 A(y_2,\tilde{y}_2)\rho(y_2)\rho(\tilde{y}_2)\left[\frac{\partial U/\partial y_2}{U^2(y_2)}\frac{\partial U/\partial \tilde{y}_2}{U^2(\tilde{y}_2)}\omega^2\right]^2\left[1-a_1\left(1+\omega\frac{\partial}{\partial\omega}\right)\right]$$
$$\times\int_0^\infty J_0\left(r\sqrt{(\omega\tau_0)^2+(k_3l_3)^2}\right)\mathrm{e}^{-\sqrt{[f(\eta_2/l_2)]^2+r^2}}r\,\mathrm{d}r. \tag{6.10}$$

And it follows from (A 14) and (A 18) of Afsar, Sescu & Leib (2016) that

$$\int_{-\infty}^{\infty}\int_{-\infty}^{\infty} \mathrm{e}^{\mathrm{i}[\omega(\tilde{\tau}-[\tilde{y}_1/U(\tilde{y}_2)-y_1/U(y_2)])-k_3\eta_3]}\langle \Gamma_\infty(\boldsymbol{y},t)\Gamma_\infty(\tilde{y}_1,\tilde{y}_2,y_3+\eta_3,t+\tilde{\tau})\rangle \,\mathrm{d}\tilde{\tau}\,\mathrm{d}\eta_3$$
$$= -2\pi\tau_0 A(y_2,\tilde{y}_2)l_3 l_2^4\rho(y_2)\rho(\tilde{y}_2)\left[\frac{\partial U/\partial y_2}{U^2(y_2)}\frac{\partial U/\partial \tilde{y}_2}{U^2(\tilde{y}_2)}\omega^2\right]^2$$
$$\times\left[1-a_1\left(1+\frac{(\omega\tau_0)^2}{\chi}\frac{\partial}{\partial\chi}\right)\right]\frac{1}{\chi}\frac{\partial}{\partial\chi}\left(\frac{\mathrm{e}^{-|f(\eta_2/l_2)|\chi}}{\chi}\right), \tag{6.11}$$

where

$$\chi\equiv\sqrt{1+(\omega\tau_0)^2+(k_3l_3)^2} \tag{6.12}$$

and (6.4) then shows that

$$S(y_2,\tilde{y}_2:k_3,\omega) = -(\rho_\infty c_\infty^2)^2\tau_0 l_2^4 l_3 A(y_2,\tilde{y}_2)\left[\frac{\mathrm{d}U}{\mathrm{d}y_2}\frac{\mathrm{d}U}{\mathrm{d}\tilde{y}_2}\frac{\omega^2}{U^3(\tilde{y}_2)U^3(y_2)}\right]$$
$$\times\left[1-a_1\left(1+\frac{(\omega\tau_0)^2}{\chi}\frac{\partial}{\partial\chi}\right)\right]\frac{1}{\chi}\frac{\partial}{\partial\chi}\left(\frac{\mathrm{e}^{-|f(\eta_2/l_2)|\chi}}{\chi}\right) \tag{6.13}$$

since ρc^2 is constant in transversely sheared flows.

7. Application to a large-aspect-ratio rectangular jet

The problem of a two-dimensional jet interacting with the trailing edge of a flat plate is currently of considerable interest because of its relevance to understanding noise production in future aircraft configurations, such as that shown in figure 3, in which the engine exhaust is of a very wide aspect ratio on an almost rectangular jet.

GAL analysed the model problem shown in figure 4 in order to represent the interaction between a jet emanating from a large-aspect-ratio rectangular nozzle with the trailing edge of a flat plate, and compared the results with recent experiments on this configuration that were performed at NASA Glenn Research Center (Zaman *et al.* 2013; Brown 2015).

They considered the general case where the mean flow is non-zero at the surface of the plate, and therefore leaves the trailing edge with different velocities above and below the interface. But, as shown below, the surface velocity is relatively small compared to the maximum velocity in the cases of interest, and will therefore be set to zero in the present computation: in which case their analysis, which minimizes the trailing-edge singularity (i.e. imposes a Kutta condition, Crighton 1985; Ayton, Gill & Peak 2016) and uses the Wiener–Hopf method to calculate the Green's function, shows that the acoustic spectrum

$$I_\omega(\boldsymbol{x})\equiv\frac{1}{2\pi}\int_{-\infty}^{\infty}\mathrm{e}^{\mathrm{i}\omega\tilde{\tau}}\overbrace{p^s(\boldsymbol{x},t)p^s(\boldsymbol{x},t+\tilde{\tau})}\,\mathrm{d}\tilde{\tau}, \tag{7.1}$$

FIGURE 3. Proposed aircraft configuration.

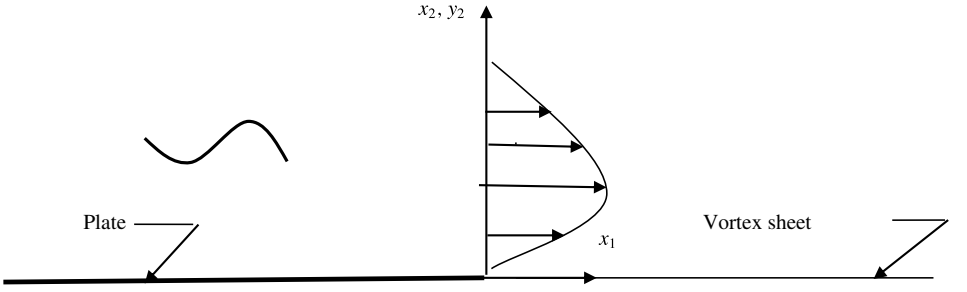

FIGURE 4. Computational model of the jet/surface interaction problem.

where $\tilde{\cdot}$ denotes the time average, is given by

$$I_\omega(\boldsymbol{x}) = \left(\frac{(2\pi)^2 k_\infty \sin\theta \sin\psi}{|\boldsymbol{x}|}\right)^2 \int_0^\infty \int_0^\infty \Phi_{\lessgtr}(k_1^{(s)}, k_3^{(s)}, y_2, \omega)\Phi^*_{\lessgtr}(k_1^{(s)}, k_3^{(s)}, \tilde{y}_2, \omega) \times \bar{G}(y_2 \mid 0 : k_3^{(s)}, \omega/U(y_2), \omega)\bar{G}^*(\tilde{y}_2 \mid 0 : k_3^{(s)}, \omega/U(\tilde{y}_2), \omega)S(y_2, \tilde{y}_2 : k_3^{(s)}, \omega)\,\mathrm{d}y_2\,\mathrm{d}\tilde{y}_2, \tag{7.2}$$

for $x_2 \lessgtr 0$ where $S(y_2, \tilde{y}_2 : k_3^{(s)}, \omega)$ is defined by (6.4),

$$k_\infty \equiv \omega/c_\infty, \tag{7.3}$$

$$k_1^{(s)} = k_\infty \cos\theta, \quad k_3^{(s)} = k_\infty \sin\theta \cos\psi, \tag{7.4a,b}$$

$$\Phi_{\lessgtr}(k_1, k_1, y_2, \omega) \equiv \frac{\kappa_-(k_1, k_3, \omega)A_{\lessgtr}}{\kappa_+(\omega/U(y_2), k_3, \omega)[\omega/U(y_2) - k_1]\hat{P}'_{\lessgtr}(0; k_1, k_3, \omega)}, \tag{7.5}$$

$$\frac{A_<}{\hat{P}'_<(0; k_1, k_3, \omega)} = \frac{1}{\sqrt{k_1^2 + k_3^2 - k_\infty^2}}, \tag{7.6}$$

$$\bar{G}(y_2 \mid 0 : k_3^{(s)}, \omega/U(y_2), \omega) = \frac{\omega^2 P_>(y_2 : \omega, \omega/U(y_2), k_3)}{(2\pi)^3 c_s^2 P'_>(0 : \omega, \omega/U(y_2), k_3)}, \tag{7.7}$$

$\kappa_\pm(k_1, k_3, \omega)$ denote bounded analytic functions in the upper/lower half-planes that satisfy the factorization condition

$$\frac{\kappa_+(k_1, k_3, \omega)}{\kappa_-(k_1, k_3, \omega)} = \frac{P_>(0 : \omega, k_1, k_3)}{P'_>(0 : \omega, k_1, k_3)} - \frac{1}{\sqrt{k_1^2 + k_3^2 - k_\infty^2}}, \tag{7.8}$$

$P_{\lessgtr}(y_2 : \omega, k_1, k_3)$ denote homogeneous solutions to (A 3) that have outgoing wave behaviour as $y_2 \to \mp\infty$, θ denotes the polar angle measured from the downstream

x_1-axis, c_s denotes the mean speed of sound at the plate surface and ψ denotes the azimuthal angle measured from the plane of the plate.

GAL considered the low-frequency limit $k_3 = O(k_\infty)$, $k_\infty \ll 1$ and obtained the result given by equation (6.33) of their paper, which has the advantage of being much more explicit than the exact $O(1)$ result but does not adequately describe the high-frequency sound field produced by the trailing-edge interaction. It does, however, adequately describe the experimentally observed low-frequency spectrum when the negative tail in the transverse velocity correlation is included (Afsar, Leib & Bozak 2017).

The high-frequency spectrum can be described by using the Wentzel–Kramers–Brillouin–Jeffreys (WKBJ) method to obtain the high-frequency outgoing wave homogeneous solution

$$P_>(y_2 : \omega, k_1, k_3) = \frac{1 - \hat{k}_1 M(y_2)}{[q(y_2 \mid \hat{k}_1, \hat{k}_3)]^{1/4}} \exp\left(\mathrm{i}k_\infty \int_0^{y_2} \sqrt{q(y \mid \hat{k}_1, \hat{k}_3)}\, \mathrm{d}y\right) \tag{7.9}$$

to (A 3) (Goldstein 1979*a*) where

$$\hat{k}_n \equiv k_n / k_\infty, \quad n = 1, 3 \tag{7.10}$$

and

$$q(y \mid \hat{k}_1, \hat{k}_3) \equiv [1 - \hat{k}_1 M(y)]^2 - \hat{k}_1^2 - \hat{k}_3^2 \tag{7.11}$$

and inserting the result into (7.5)–(7.8) to obtain the following

$$\frac{\kappa_+(k_1, k_3, \omega)}{\kappa_-(k_1, k_3, \omega)} = \frac{-2}{\sqrt{k_1^2 + k_3^2 - k_\infty^2}}, \tag{7.12}$$

$$\kappa_-(k_1, k_3, \omega) = -\tfrac{1}{2}\sqrt{k_1 - k_\infty(1 - \sin^2\theta \cos^2\psi)^{1/2}}, \tag{7.13}$$

$$\kappa_+(k_1, k_3, \omega) = \frac{1}{\sqrt{k_1 + k_\infty(1 - \sin^2\theta \cos^2\psi)^{1/2}}}. \tag{7.14}$$

It, therefore, follows that

$$\Phi_<(k_1^{(s)}, k_1^{(s)}, y_2, \omega) = \frac{-M^{1/2}(y_2)\sqrt{1 + \beta M(y_2)}}{2k_\infty[1 - M(y_2)\cos\theta]\sqrt{\beta + \cos\theta}} \tag{7.15}$$

and

$$\bar{G}(y_2 \mid 0 : k_3^{(s)}, \omega/U(y_2), \omega) = \frac{-\mathrm{i}k_\infty \exp\left(\mathrm{i}k_\infty \int_0^{y_2} \sqrt{q(y \mid y_2)}\, \mathrm{d}y\right)}{(2\pi)^3 [q(0 \mid y_2) q(y_2 \mid y_2)]^{1/4}}, \tag{7.16}$$

where

$$q(y \mid y_2) \equiv q(y \mid 1/M(y_2), \sin\theta \cos\psi) \tag{7.17}$$

and (7.2) then becomes

$$I_\omega(\boldsymbol{x}) = \left(\frac{k_\infty}{4\pi|\boldsymbol{x}|}\right)^2 (\beta - \cos\theta) \int_0^\infty \int_0^\infty \frac{[M(y_2)M(\tilde{y}_2)]^{3/2} Q(y_2|\theta, \varphi)[Q(\tilde{y}_2|\theta, \varphi)]^*}{[1 - M(y_2)\cos\theta][1 - M(\tilde{y}_2)\cos\theta]} \times \frac{S(y_2, \tilde{y}_2 : k_3^{(s)}, \omega)}{\sqrt{[1 - \beta M(y_2)][1 - \beta M(\tilde{y}_2)]}}\, \mathrm{d}y_2\, \mathrm{d}\tilde{y}_2, \tag{7.18}$$

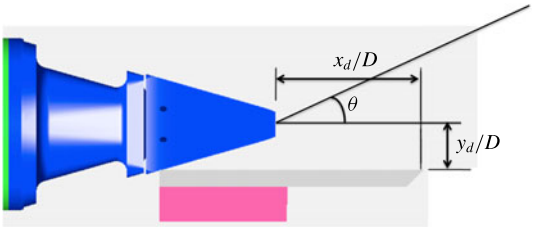

FIGURE 5. Nozzle/plate configuration. Figure courtesy Dr James E. Bridges, NASA Glenn.

for $x_2 < 0$ where

$$Q(y_2 \mid \theta, \varphi) \equiv \left[\frac{q(0 \mid y_2) - \mathrm{e}^{-\chi_0 k_\infty}}{q(y_2 \mid y_2)}\right]^{1/4} \exp\left(\mathrm{i}k_\infty \int_0^{y_2} \sqrt{q(y \mid y_2)}\,\mathrm{d}y\right)^2, \tag{7.19}$$

$$\beta \equiv (1 - \sin^2\theta \cos^2\psi)^{1/2}, \tag{7.20}$$

$M(y_2) = U(y_2)/c_\infty$ denotes the local acoustic Mach number at the position y_2, χ_0 is a positive constant and we have inserted the exponential damping factor $\mathrm{e}^{-\chi_0 k_\infty}$ into (7.19), which leaves the asymptotic expansion unchanged to the order of approximation considered here. In other words, it is asymptotically equivalent to the straightforward result. It reduces to the low-frequency result (6.33) of GAL when $Q(y_2 \mid \theta, \varphi) = 1$. But $Q(y_2 \mid \theta, \varphi)$ also $\to 1$ as $k_\infty \to 0$ and (7.18), therefore, behaves like (but is not identical to) a uniformly valid composite solution that applies at all frequencies.

It is, of course necessary to insert a formula for the source function S into (7.18) before using these results to calculate the acoustic field. GAL used a rather complicated approximate procedure to relate this quantity to an experimentally measurable turbulence correlation. The present analysis allows us to use the much simpler and more general exact relation (6.4), and model the turbulence correlation to obtain the explicit formula (6.13) for S.

As indicated above, the model problem considered in this section can be used to represent the interaction between a jet emanating from a large-aspect-ratio rectangular nozzle with the trailing edge of a flat plate. The analysis is basically inviscid, but accounts for viscous effects by imposing a Kutta condition at the trailing edge (GAL). Brown & Daniels (1975) use high-Reynolds-number asymptotic analysis to show that this condition is consistent with the viscous boundary layer flow at the trailing edge. The importance of imposing a Kutta condition in inviscid analyses involving an edge has been reviewed and discussed by Crighton (1985) and Ayton *et al.* (2016).

Recent experiments on this configuration were performed at NASA Glenn Research Center (Zaman *et al.* 2013; Brown 2015). The relevant geometric parameters are shown in figure 5.

We assume that the mean density ρ is constant and the mean velocity profile $U(y_2)$ can be represented by the twice differentiable function

$$U(y_2) = U_d \begin{cases} \left[\dfrac{(t_d/2)^2 - (y_2 - y_d)^2}{(t_d/2)^2}\right]^2 \mathrm{e}^{-(y_2 - y_d)^2\kappa^2}, & \text{for } (y_2 - y_d)^2 < (t_d/2)^2 \\ 0, & \text{for } (y_2 - y_d)^2 > (t_d/2)^2, \end{cases} \tag{7.21}$$

with compact support $|y_2 - y_d| \leqslant t_d/2$, where y_d is the distance from the plate to the nozzle centreline (see figure 5), t_d is the thickness of the jet and κ controls the profile decay.

Since the factor $A(y_2, \tilde{y}_2)$ in (6.8) must vanish at the jet boundaries and is determined by strength of the turbulence at the source location, we expect $A(y_2, y_2)$ to be proportional to the turbulence intensity at y_2, which is roughly proportional to the mean velocity gradient at that point. We therefore set

$$A(y_2, \tilde{y}_2) \equiv A_0 \sqrt{|\mathrm{d}U(y_2)/\mathrm{d}y_2||\mathrm{d}U(\tilde{y}_2)/\mathrm{d}\tilde{y}_2|}[\alpha(y_2)\alpha(\tilde{y}_2)] + B_0 U(y_2)U(\tilde{y}_2), \tag{7.22}$$

where B_0 and A_0 are constants and the factor

$$\alpha(y_2) = \begin{cases} [(t_d/2)^2 - (y_2 - y_d)^2]^3, & \text{for } (y_2 - y_d)^2 < (t_d/2)^2 \\ 0, & \text{for } (y_2 - y_d)^2 > (t_d/2)^2 \end{cases} \tag{7.23}$$

is inserted to ensure that the turbulence correlation (6.9) vanishes at the jet boundaries.

Measurements of the noise generated by the interaction of rectangular jets in the vicinity of a flat-plate trailing edge have been carried out at NASA Glenn Research Center (Bridges *et al.* 2014; Brown 2015) in a facility validated for jet noise (Bridges & Brown 2005; Brown & Bridges 2006). Flow measurements for essentially the same geometries, but at a lower jet exit Mach number ($M_a = 0.22$), were carried out by Zaman *et al.* (2013). We chose the configuration where the plate was located at 1.2 equivalent diameters from the jet centreline and 5.7 equivalent diameters downstream of the exit of an 8 : 1 rectangular nozzle, for jet exit acoustic Mach numbers $M_a =$ 0.5, 0.7, 0.9 as test cases for the theory. The arbitrary length scale D was taken to be an equivalent nozzle diameter defined by $\pi(D/2)^2 =$ nozzle width $\times$ nozzle height with nozzle width $= 8 \times$ nozzle height, and was approximately equal to 2.12 inches in the experiments. Any 'scrubbing noise' that may have resulted from the flow along the plate was deemed to be negligible for this configuration (Khavaran, Bozak & Brown 2016). Recall that the source location is assumed to be at a large distance from edge and independent of its location on the scale of the interaction, but not on the longer scale over which the turbulence and mean flow evolve. So the mean flow and turbulence properties must be recalibrated when changes in edge location occur on the latter scale.

Figure 6(*a*) shows a comparison of the normalized (by the jet exit velocity, U_J) mean velocity profile from the model (7.21) with velocity measurements at a very small distance downstream of the plate trailing edge carried out by Zaman *et al.* (2013). Reynolds-averaged Navier–Stokes solutions for the test cases considered in this paper (Afsar *et al.* 2017) show that the normalized mean velocity profiles for $M_a = 0.5$, 0.7, 0.9 are similar to each other and to that measured by Zaman *et al.* (2013) at $M_a = 0.22$. (There is a very slight mismatch in the transverse distance of the plate to the nozzle centreline between the Zaman *et al.* (2013) experiment and the one where the acoustic data were taken, which may partially account for the slightly higher velocity at $y_2/D_J = 0$.) We therefore use the same normalized mean flow model for all jet exit velocities with the mean flow parameters for a best fit to the data, as indicated in the caption of figure 6. The data show that the mean velocity is small but not equal to zero at the interface. This can, in part, be attributed to the turbulent mixing that occurs upstream of the measuring station which, as noted above, was located slightly downstream of the trailing edge. But as pointed out by one of the referees, it could also be due to weakly nonlinear velocity fluctuations, which

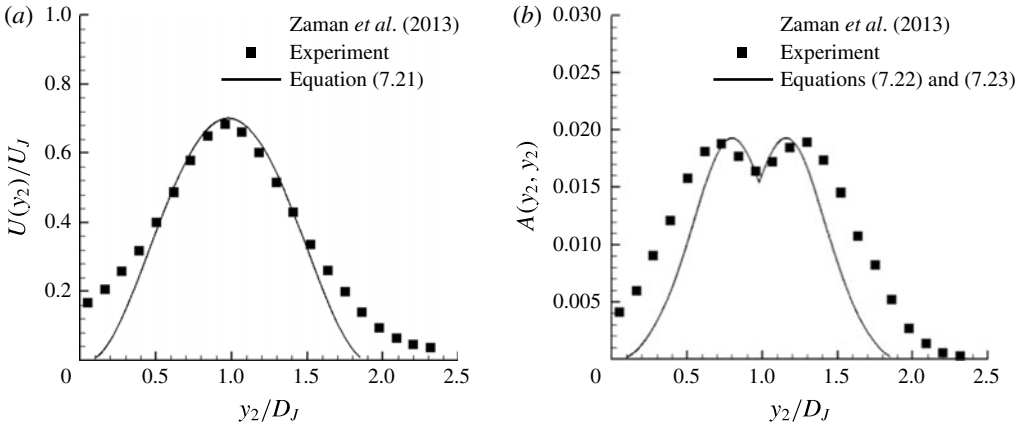

FIGURE 6. Comparison of (*a*) mean velocity profile and (*b*) turbulent kinetic energy calculated from (7.21) and (7.22) against experiments reported in Zaman *et al.* (2013). $(y_d, t_d) = (0.98, 1.85)$, $\kappa = 0.2$ and $(A_0, B_0) = (0.011, 0.022)$.

causes the mean velocity to leave the trailing edge at different speeds above and below the plate. Hunt *et al.* (2016) have recently shown that the mean speeds above and below the trailing edge can differ if the plate is at a small angle to the mean flow, and similar effects could occur in the present case where it is nominally aligned with the flow. However, the interface velocity is relatively small and in our cases is deemed to be insignificant relative to other uncertainties in the data comparisons.

Figure 6(*b*) compares the turbulent kinetic energy measurements from the same experiment to the amplitude $A(y_2, y_2)$ defined by (7.22) and (7.23) with the parameters A_0 and B_0 set equal to 0.011 and 0.022, respectively. The normalized turbulent kinetic energy profiles are also relatively independent of jet exit velocity (Afsar *et al.* 2017), and the models appear to be in reasonable agreement with the flow data. They are therefore used in the following noise predictions.

Numerical results for the noise generated by jet–edge interaction are obtained by evaluating the formula (7.18) for the acoustic spectrum, with the double integrals being computed using a standard Simpson's method. The integrand in (7.18) vanishes outside of the support of the mean flow function (7.21), and the range of integration in this equation is therefore limited to the region where $U(y_2) \neq 0$.

Figures 8–10 show quantitative comparisons of measurements of the far-field pressure fluctuations' power spectral density per unit Strouhal number $= fD/U_J$, in dB scale $PSD = 10\log(4\pi I_\omega U_J/Dp_{ref}^2)$ (referenced to $p_{ref} = 20$ μPa) taken by Brown (2015) with predictions obtained by inserting the spectrum (6.13) with $f = |\eta_2/l_2| = |(y_2 - \tilde{y}_2)/l_2|$ into the composite RDT solution (7.18). Results are shown at observer locations directly below the plate ($\psi = -90°$) and at several observer polar angles, θ, measured from the downstream jet axis. The experimental trailing-edge noise was educed by subtracting the noise measured in the corresponding free jet (i.e. in the absence of a plate) from the total measured noise. The parameters used in the predictions shown in figures 8–10 are $\tau_0 = 2.5$ and $(l_2, l_3) = (0.67, 0.25)$, $\chi_0 = 1$. Setting the coefficient a_1 equal to 0.75 in (6.8) produces a normalized turbulence correlation $\langle U_\perp(t - y_1/U(y_2), \boldsymbol{y}_T)U_\perp(t + \tilde{\tau} - y_1/U(y_2), \tilde{y}_2, y_2 + \eta)\rangle$, shown in figure 7, which exhibits the experimentally observed cusp behaviour at zero spatial and temporal separations (figure 7*b*) and the small but definite negative region at larger time delays.

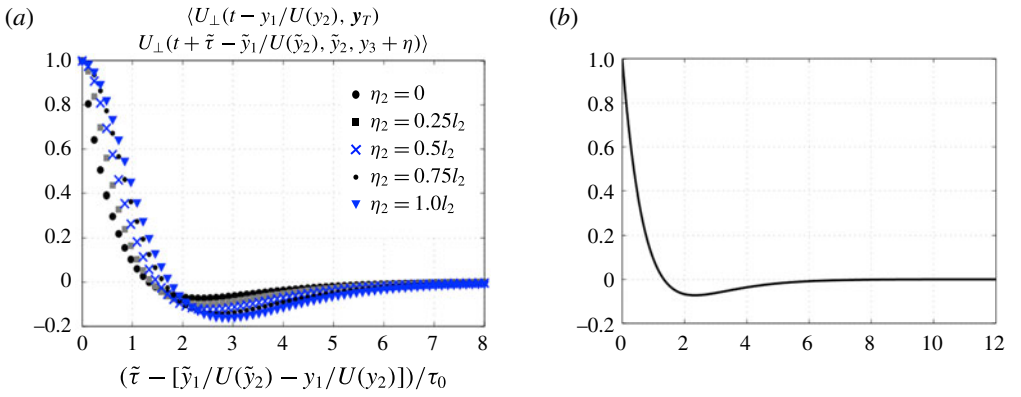

FIGURE 7. (Colour online) Normalized transverse turbulence correlation (6.8) at $\eta_3 = 0$ with parameters $\tau_0 = 2.5$, $(l_1, l_2) = (0.67, 0.25)$ and $a_1 = 0.75$ (*a*) various fixed η_2 (*b*) $\eta_2 = 0$.

The results for the downstream polar angles (in figures 8–10) show that the present RDT-based edge-noise predictions are in much better agreement with the data than those given in Goldstein *et al.* (2013*a*) and Afsar *et al.* (2017). The agreement is now very good over the entire frequency range where the total measured noise (red symbols) is dominated by that generated by the jet–surface interaction alone (green symbols) for all jet exit Mach numbers at the downstream polar angles shown. The results of GAL were limited to $St < 0.4$ and $Ma >= 0.7$. The predictions shown in figure 11 for upstream polar angles are also in very good agreement over the entire Mach number range.

Figure 12 is a comparison of the acoustic predictions obtained by inserting the present source function model (6.13) into the low-frequency solution used in GAL and Afsar *et al.* (2017) for the parameter values used in figures 8–10. As expected, the present approach converges to the low-frequency result at very low frequencies and, therefore, represents a much more robust mathematical model of trailing-edge noise than either of the two previous studies since (for reasons indicated below (7.20)) it is now applicable to $O(1)$ frequencies. And our numerical tests show that the low-frequency roll-off is now much less sensitive to the magnitude of the negative loop in the correlation function $\langle U_\perp(t - y_1/U(y_2), \boldsymbol{y}_T)U_\perp(t + \tilde{\tau} - y_1/U(y_2), \tilde{y}_2, y_2 + \eta)\rangle$ than the Afsar *et al.* (2017) model – although it is necessary to include this feature in the model in order for the transverse turbulence correlation to be physically realizable. In the present model the negative (anticorrelation) region enables the correct prediction of the absolute level of the very low frequency sound (i.e. for $St < 0.1$) rather than the roll-off *per se.*

The improved predictions of the present result (relative to that obtained in GAL) is largely due to the $\exp(\mathrm{i}k_\infty \int_0^{y_2} \sqrt{q(y \mid y_2)}\,\mathrm{d}y)$ factor in (7.19), which damps out the high frequencies and, therefore, increases the high-frequency roll-off, since the argument of the exponential $\mathrm{i}k_\infty \int_0^{y_2} \sqrt{q(y \mid y_2)}\,\mathrm{d}y$ is always negative. It accounts for the bending of the sound waves away from the downstream axis and, therefore, represents a kind of 'zone of silence'.

The present calculations are based on (6.4), which is obtained by using causality to interpret the singular integral (4.13) for the transverse particle displacement $\eta_\perp(\boldsymbol{y}, \tau)$. But the causality condition results from an initial condition imposed in the distant past and, as argued in the introduction, the long-time solutions to the initial value

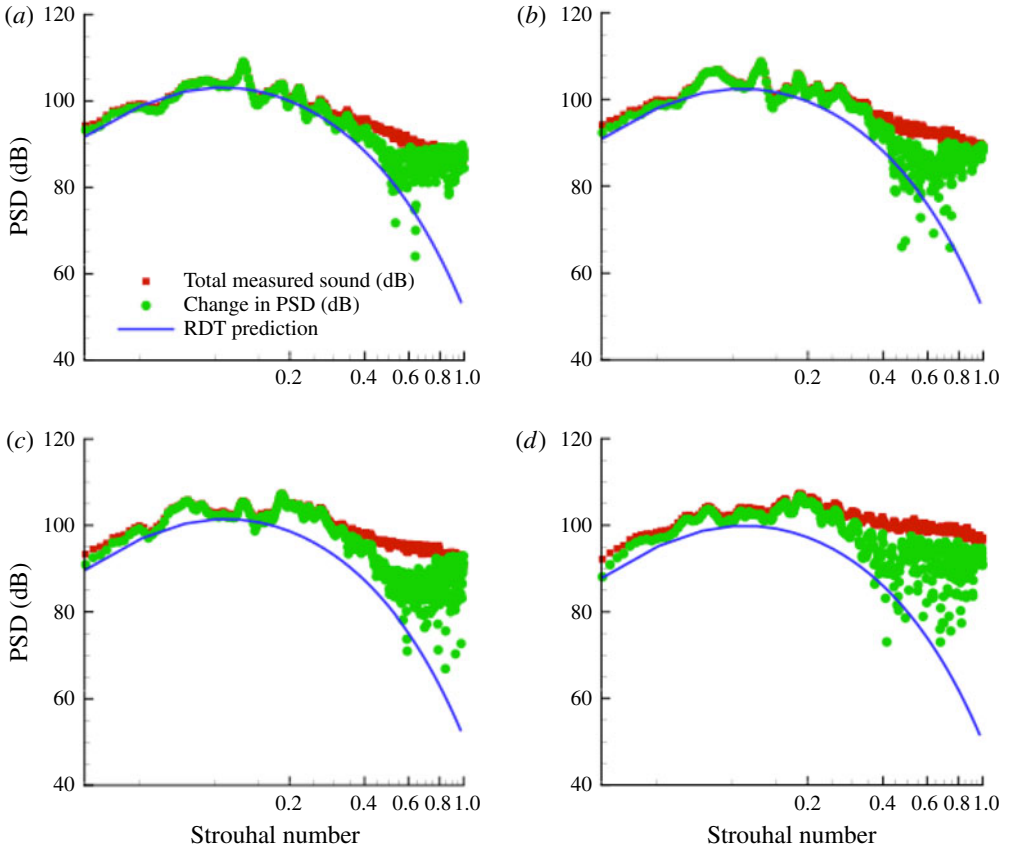

FIGURE 8. Power spectral density (PSD) of the far-field pressure fluctuations at 100 equivalent diameters from nozzle exit (lossless in dB scale referenced to 20 μPa) as a function of Strouhal number, for $M_a = 0.9$. Predicted (solid line): measured data below the plate at $\psi = -90°$. (Total noise: red; difference between the total noise and noise measured in the free jet: green.) Plate trailing edge at $(x_d, y_d)/D = (5.7, 0.98)$. (*a*) $\theta = 90°$, (*b*) $\theta = 75°$, (*c*) $\theta = 60°$, (*d*) $\theta = 45°$.

problem are not necessarily relevant to the time-stationary turbulent flows being considered here. (Similar arguments can be found in Mani 1976; Dowling, Ffowcs Williams & Goldstein 1978.) However, the singular integral in (4.13) will also be well defined if it is interpreted as a Cauchy principal value. The resulting formulae turn out to be more complicated than the present results, and our computations (not shown here) indicate that the acoustic predictions based on these formulae do not differ significantly from the present results – at least in the low-frequency limit where comparisons were carried out. Data comparisons, such as those given in this section, therefore, cannot be used to distinguish between the two approaches.

Figures 8–10 show that the predictions are better for larger polar angles (near ninety degrees) and higher Mach numbers, as they were in GAL and Afsar *et al.* (2017). The former is due to reduction in edge noise relative to the jet noise for shallow polar observation angles and the latter (the deterioration in prediction for $M_a = 0.5$ near $St \sim 0.1$) may be a particular feature of the experimental data (Bridges 2014) or may be associated with a change in the interference between

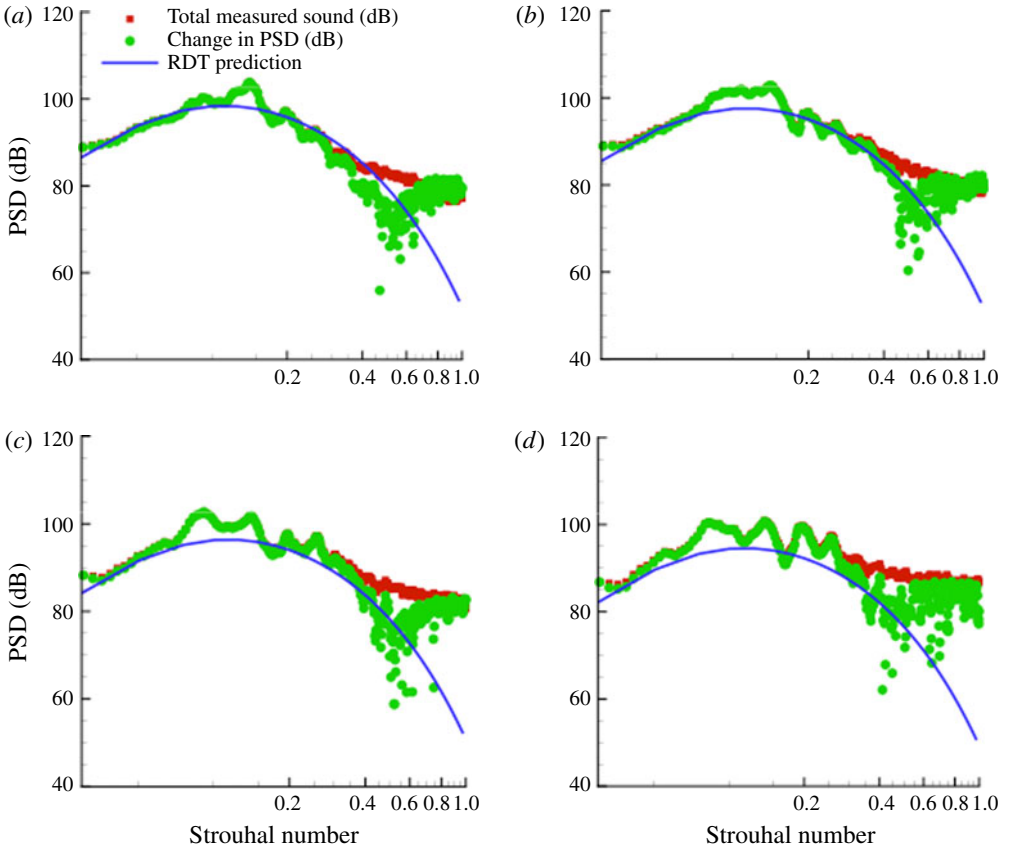

FIGURE 9. Power spectral density (PSD) of the far-field pressure fluctuations at 100 equivalent diameters from nozzle exit (lossless in dB scale referenced to 20 μPa) as a function of Strouhal number, for $M_a = 0.7$. Predicted (solid line): measured data below the plate at $\psi = -90°$. (Total noise: red; difference between the total noise and noise measured in the free jet: green.) Plate trailing edge at $(x_d, y_d)/D = (5.7, 0.98)$. (*a*) $\theta = 90°$, (*b*) $\theta = 75°$, (*c*) $\theta = 60°$, (*d*) $\theta = 45°$.

the non-convecting jet noise and edge noise (Afsar *et al.* 2017, p. 202) at lower Mach numbers. There are four free parameters: (l_2, l_3, τ_0, a_1) that determine the source function S in the present model, with all other parameters determined by matching to the turbulence or mean flow data, which makes the predictions much less empirical than those of GAL and Afsar *et al.* (2017). No empirical coefficients would be required if there were an experimental database for the transverse velocity correlation $\langle U_\perp(t - y_1/U(y_2), \boldsymbol{y}_T)U_\perp(t + \tilde{\tau} - y_1/U(y_2), \tilde{y}_2, y_2 + \eta)\rangle$ for a rectilinear jet in the vicinity of a plate trailing edge. It could also be obtained computationally using large eddy simulation (LES) which would be much less expensive than a jet-noise experiment. The parameters could, in principle, also be obtained by further optimizing the agreement with the measured spectra.

8. Concluding remarks

This paper is based on the formal solutions (2.14)–(2.16) to the linearized Euler equations for transversely sheared mean flows which, like the Kovasznay results for

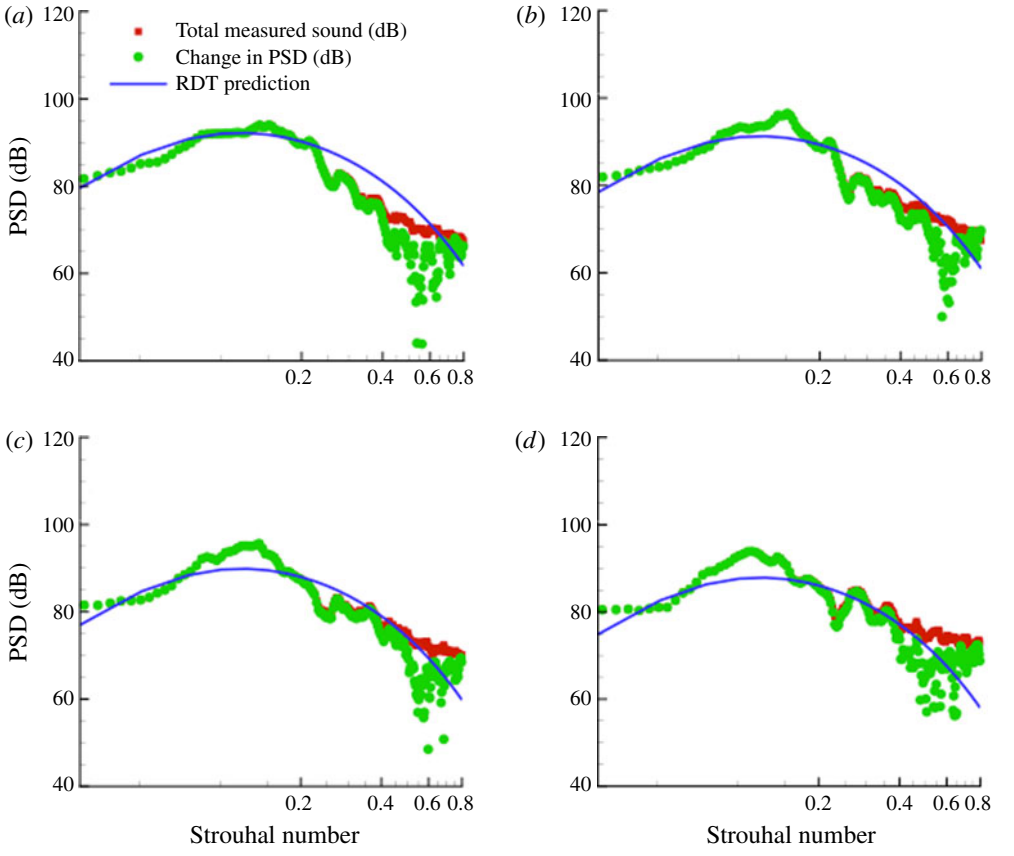

FIGURE 10. Power spectral density (PSD) of the far-field pressure fluctuations at 100 equivalent diameters from nozzle exit (lossless in dB scale referenced to 20 μPa) as a function of Strouhal number, for $M_a = 0.5$. Predicted (solid line): measured data below the plate at $\psi = -90°$. (Total noise: red; difference between the total noise and noise measured in the free jet: green). Plate trailing edge at $(x_d, y_d)/D = (5.7, 0.98)$. (*a*) $\theta = 90°$, (*b*) $\theta = 75°$ (*c*) $\theta = 60°$ (*d*) $\theta = 45°$.

the unsteady motion on uniform flows, involve two arbitrary convected quantities $\vartheta(\tau - y_1/U, \boldsymbol{y}_T)$ and $\tilde{\omega}_c(\tau - y_1/U, \boldsymbol{y}_T)$ that can be associated with the hydrodynamic component of the flow and can, therefore, be used to specify upstream boundary (i.e. initial) conditions for RDT problems that involve the interaction of turbulence with solid surfaces. This paper derives a new relation between these quantities and the physically measurable variables that is much simpler and more general than the one given in Goldstein *et al.* (2013*a*,*b*).

This relation was used to relate the source term S that appears in the formula (7.2) for the noise generated by the interaction of a two-dimensional jet with a semi-infinite flat plate derived in Goldstein *et al.* (2013*a*) to the physically measurable second-order velocity correlations in the jet. The result was combined with a modified high-frequency solution to obtain a specific formula for the acoustic spectrum that applies over a broad range of frequencies. This result was then compared with experimental measurements carried out at Glenn Research Center, and excellent agreement was obtained. The general results can of course, be applied to many other RDT problems

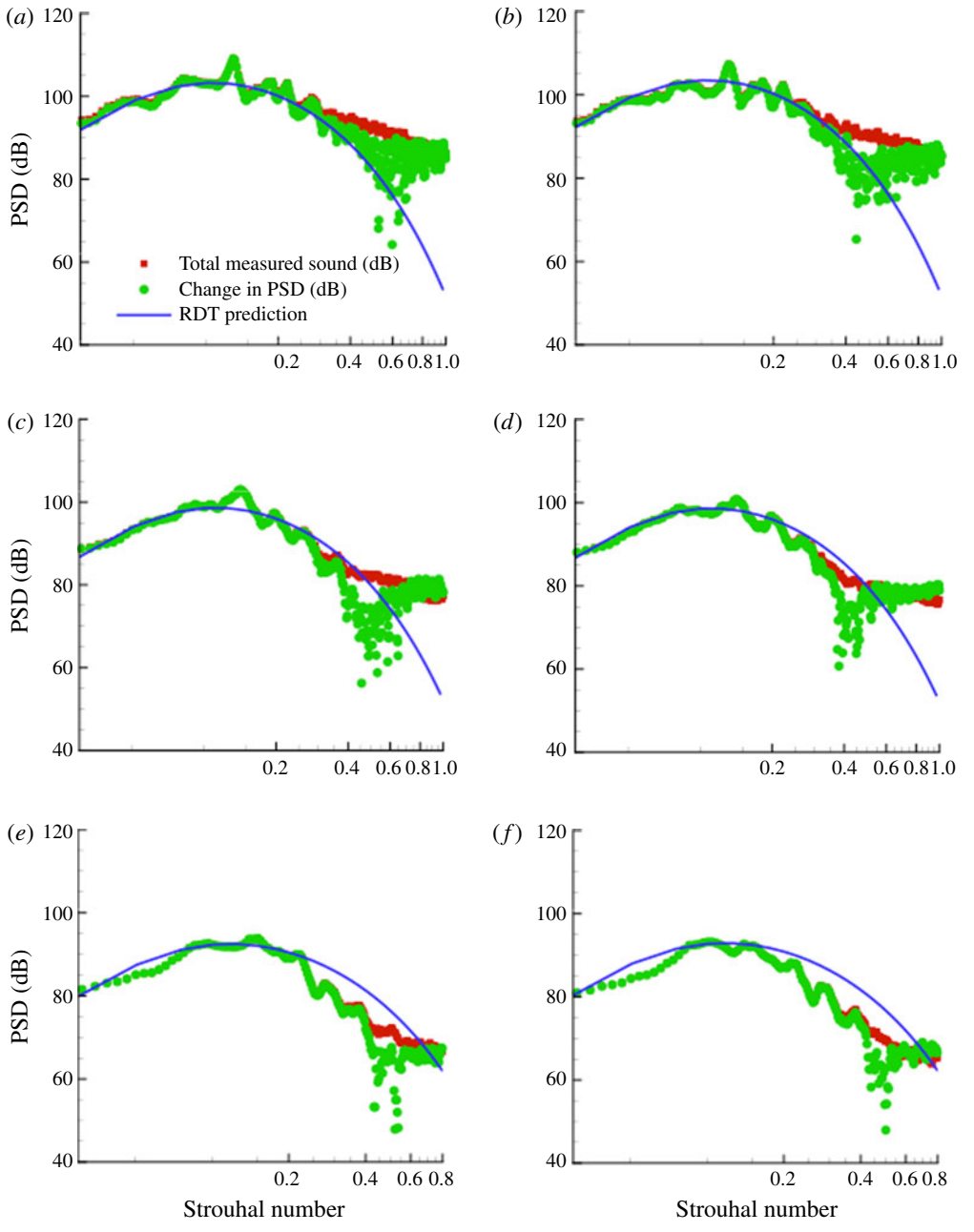

FIGURE 11. Power spectral density (PSD) of the far-field pressure fluctuations at 100 equivalent diameters from nozzle exit (lossless in dB scale referenced to 20 μPa) as a function of Strouhal number. Predicted (solid line): measured data below the plate at $\psi = -90°$. (Total noise: red; difference between the total noise and noise measured in the free jet: green.) For plate trailing edge at $(x_d, y_d)/D = (5.7, 0.98)$. (*a*) $M_a = 0.9$, $\theta = 95°$, (*b*) $M_a = 0.9$, $\theta = 105°$, (*c*) $M_a = 0.7$, $\theta = 95°$, (*d*) $M_a = 0.7$, $\theta = 105°$, (*e*) $M_a = 0.5$, $\theta = 95°$, (*f*) $M_a = 0.5$, $\theta = 105°$.

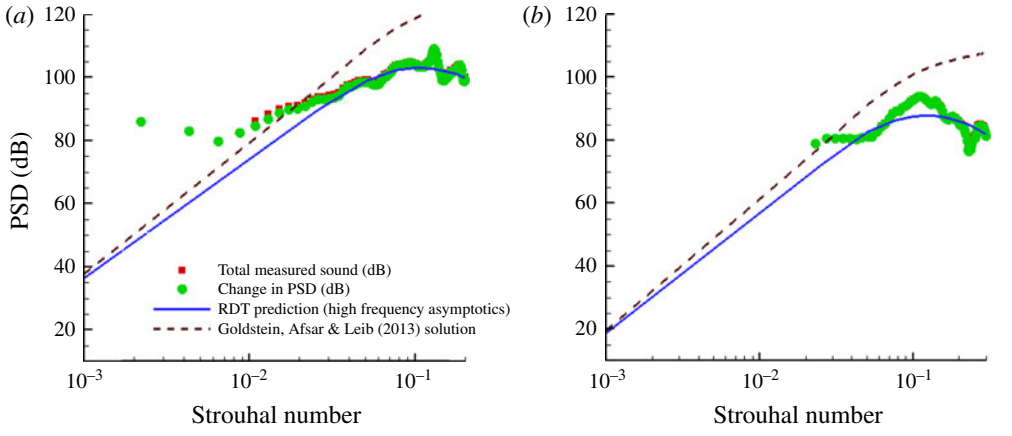

FIGURE 12. Convergence to the GAL solution. Same legend as figures 8–11. (*a*) $M_a = 0.9, \theta = 90°$, (*b*) $M_a = 0.5, \theta = 45°$.

involving the interaction of turbulence with surfaces embedded in transversely sheared base flows or, more generally, in vortical base flows that asymptote to transversely sheared mean flows in the upstream region.

Acknowledgements

The authors would like to thank Drs K. Zaman, J. Bridges and C. Brown for providing their experimental data and their helpful comments. This work was supported by the NASA Advanced Air Vehicles Program, Commercial Supersonic Technology Project. M.Z.A. would also like to thank Strathclyde University for financial support from the Chancellor's Fellowship.

Appendix A. Green's function for 2-D base flow

Since $\bar{G}_0(\boldsymbol{y}_T \,|\, \boldsymbol{x}_T : \omega, k_1)$ can only depend on x_3 and y_3 in the combination $x_3 - y_3$, for the planar mean flow

$$U = U(y_2), \quad c = c(y_2) \tag{A 1a,b}$$

the reduced Green's function

$$\hat{G}(y_2 \,|\, x_2 : \omega, k_1, \hat{k}) \equiv \frac{1}{2\pi} \int_{-\infty}^{\infty} \mathrm{e}^{\mathrm{i}(y_3 - x_3)\hat{k}} \bar{G}_0(\boldsymbol{y}_T \,|\, \boldsymbol{x}_T : \omega, k_1)\, \mathrm{d}(y_3 - x_3) \tag{A 2}$$

only depends on the indicated arguments and satisfies the reduced Rayleigh equation

$$\frac{\mathrm{d}}{\mathrm{d}y_2}\left\{\frac{c^2(y_2)}{[\omega - U(y_2)k_1]^2}\frac{\mathrm{d}\hat{G}}{\mathrm{d}y_2}\right\} + \left\{1 - \frac{c^2(y_2)}{[\omega - U(y_2)k_1]^2}(k_1^2 + k_3^2)\right\}\hat{G} = \frac{\delta(x_2 - y_2)}{(2\pi)^3}, \tag{A 3}$$

whose solution is given by

$$\hat{G}(y_2 \,|\, x_2) = \hat{G}(x_2 \,|\, y_2) = \frac{\hat{P}_{\pm}(y_2)\hat{P}_{\mp}(x_2)}{\Delta(k_1, k_3, \omega)} \quad \text{for } y_2 > / < x_2, \tag{A 4}$$

where $\hat{P}_+(y_2), \hat{P}_-(y_2)$ are the homogeneous solutions of (A 3) that exhibit appropriate boundary conditions at the outer/inner edges of the shear layer and, according to Abel's theorem,

$$\Delta(\omega, k_1, k_3) \equiv -\frac{(2\pi)^3 c^2[\hat{P}_+(y_2)\hat{P}'_-(y_2) - \hat{P}_-(y_2)\hat{P}'_+(y_2)]}{[\omega - U(y_2)k_1]^2} \tag{A 5}$$

depends on the normalization of $\hat{P}_+(y_2), \hat{P}_-(y_2)$ but is independent of y_2, which means that the reduced transverse velocity Green's function

$$\hat{G}_2(y_2 \,|\, x_2 : \omega, k_1, k_3) = \frac{1}{2\pi}\int_{-\infty}^{\infty} \mathrm{e}^{-\mathrm{i}k_3((y_3 - x_3))}\bar{G}_2(\boldsymbol{y}_T \,|\, \boldsymbol{x}_T : \omega, k_1)\,\mathrm{d}(y_3 - x_3), \tag{A 6}$$

where $\bar{G}_2(\boldsymbol{y}_T \,|\, \boldsymbol{x}_T : \omega, k_1)$ is defined by (4.9), only depends on the indicated argument and is given by

$$\hat{G}_2(y_2 \,|\, x_2) = \frac{1}{[\mathrm{i}k_1 U(x_2) - \mathrm{i}\omega]}\frac{\partial}{\partial x_2}\frac{\hat{P}_\pm(y_2)P_\mp(x_2)}{\Delta(k_1, k_3, \omega)} \quad \text{for } y_2 > / < x_2. \tag{A 7}$$

So the limit

$$\lim_{k_1 \to \omega/U(y_2)} \Delta(k_1, k_3, \omega) \tag{A 8}$$

is expected to exist and be non-zero except at perhaps at a finite number of points, say $y_2 = y_2^{(n)}(\omega)$, for $n = 1, 2, \ldots$ for any value of k_3, ω. This also shows that $\hat{G}_2(y_2 \,|\, x_2 : \omega, \omega/U(y_2)k_3)$ and, therefore, $\bar{G}_2(\boldsymbol{y}_T \,|\, \boldsymbol{x}_T : \omega, \omega/U(y_2))$ must be continuous at $x_2 = y_2$. Moreover, it follows from the method of Frobenius that (A 3) possesses two linearly independent solutions, say $\hat{P}_1(y_2), \hat{P}_2(y_2)$, that behave like

$$\hat{P}_1(y_2) = O((\omega - k_1 U(y_2))^3) = O((y_2 - y_2^{(0)})^3), \tag{A 9}$$

$$\hat{P}_2(y_2) = a + b(\omega - k_1 U(y_2))^2 + c\hat{P}_1(y_2)\ln(\omega - k_1 U(y_2)) + O((y_2 - y_2^{(0)})^3), \tag{A 10}$$

as $y_2 \to y_2^{(0)}$, where $y_2^{(0)}$ is a point where $U(y_2^{(0)}) = \omega/k_1$ and a, b, c are constants. So

$$\lim_{\substack{k_1 \to \omega/U(y_2) \\ y_2 = \text{const.}}} \{\hat{P}_+(y_2 : k_1, k_3, \omega), \hat{P}_-(y_2 : k_1, k_3, \omega)\}$$

$$= \lim_{\substack{y_2 \to y_2^{(0)} \\ y_2^{(0)} = \text{const.}}} \{\hat{P}_+(y_2 : \omega/U(y_2^{(0)}), k_3, \omega), \hat{P}_-(y_2 : \omega/U(y_2^{(0)}), k_3, \omega)\} \tag{A 11}$$

is also expected to exist and be non-zero since $\hat{P}_+(y_2)$, $\hat{P}_-(y_2)$ must be linear combinations of $\hat{P}_1(y_2)$, $\hat{P}_2(y_2)$. It, therefore, follows from (A 2) and (A 4) that the limits

$$\bar{G}_0(\boldsymbol{y}_T \,|\, \boldsymbol{x}_T : \omega, \omega/U(\boldsymbol{y}_T)) \equiv \lim_{k_1 \to \omega/U(\boldsymbol{y}_T)} \bar{G}_0(\boldsymbol{y}_T \,|\, \boldsymbol{x}_T : \omega, k_1) \tag{A 12}$$

and

$$\bar{G}_i(\boldsymbol{y}_T \,|\, \boldsymbol{x}_T : \omega, \omega/U(\boldsymbol{y}_T)) \equiv \lim_{k_1 \to \omega/U(\boldsymbol{y}_T)} \bar{G}_i(\boldsymbol{y}_T \,|\, \boldsymbol{x}_T : \omega, k_1) \tag{A 13}$$

also exists and are non-zero everywhere except at the finite number of points where $\Delta(k_1, k_2, \omega)$ is equal to zero.

Appendix B. Behaviour of transverse velocity at upstream infinity

When the mean flow is two-dimensional the integral

$$I_i \equiv \int_{A_T} \mathrm{e}^{\mathrm{i}\omega x_1/U(y_T)} \bar{G}_i(\boldsymbol{y}_T \,|\, \boldsymbol{x}_T : \omega, \omega/U(\boldsymbol{y}_T)) \bar{\Omega}_c(\boldsymbol{y}_T : \omega)\, \mathrm{d}\boldsymbol{y}_T \tag{B 1}$$

on the right-hand side of (4.3) can be written as

$$I_2(\boldsymbol{x} : \omega) = \int_{-\infty}^{\infty} \int_{y_0}^{\infty} \mathrm{e}^{\mathrm{i}\omega x_1/U(y_2)} \bar{G}_2(y_2, y_3 \,|\, x_2, x_3 : \omega, \omega/U(y_2)) \bar{\Omega}_c(y_2, y_3 : \omega)\, \mathrm{d}y_2\, \mathrm{d}y_3, \tag{B 2}$$

where y_0 can be set to $-\infty$ if the cross-sectional A_T is all of space and can be set to zero if the flow is bounded by an inner surface that extends from $y_1 = -\infty$ to $y_1 = +\infty$. Now suppose that

$$\bar{\Omega}_c(y_2, y_3 : \omega) = O([U'(y_2)]^3) \tag{B 3}$$

whenever $U'(y_2) \to 0$. (We shall verify that $\bar{\Omega}_c(y_2, y_3 : \omega)$ actually exhibits this behaviour after the fact.) Then, since $\bar{G}_2(y_2, y_3 \,|\, x_2, x_3 : \omega, \omega/U(y_2))$ is continuous at $y_2 = x_2$, and $U^2(y_2)/U'(y_2)$ times the integrand and $U^2(y_2)/U'(y_2)$ times the derivative of this quantity are expected to vanish at the end points y_0, ∞, equation, (B 2) can be integrated by parts twice from y_0 to x_2 and from x_2 to ∞ to show that

$$\begin{aligned}
I_2 \;\equiv\; & \frac{1}{\mathrm{i}\omega x_1} \int_{-\infty}^{\infty} \int_{y_0}^{\infty} \mathrm{e}^{\mathrm{i}\omega x_1/U(y_2)} \frac{\partial}{\partial y_2} \\
& \times \left[\frac{U^2(y_2)}{U'(y_2)} \bar{G}_2(y_2, y_3 \,|\, x_2, x_3 : \omega, \omega/U(y_2)) \bar{\Omega}_c(y_2, y_3 : \omega) \right] \mathrm{d}y_2\, \mathrm{d}y_3 \\
= \; & -\mathrm{e}^{\mathrm{i}\omega x_1/U(x_2)} \left[\frac{U^2(x_2)}{\omega x_1 U'(x_2)} \right]^2 \\
& \times \int_{-\infty}^{\infty} \Delta \left[\frac{\partial}{\partial x_2} \bar{G}_2(x_2, y_3 \,|\, x_2, x_3 : \omega, \omega/U(x_2)) \right] \bar{\Omega}_c(x_2, y_3 : \omega)\, \mathrm{d}y_3 \\
& - \frac{1}{(\omega x_1)^2} \int_{-\infty}^{\infty} \int_{y_0}^{\infty} \mathrm{e}^{\mathrm{i}\omega x_1/U(y_2)} \frac{\partial}{\partial y_2} \\
& \times \left\{ \frac{U^2(y_2)}{U'(y_2)} \frac{\partial}{\partial y_2} \left[\frac{U^2(y_2)}{U'(y_2)} \bar{G}_2(y_2, y_3 \,|\, x_2, x_3 : \omega, \omega/U(y_2)) \bar{\Omega}_c(y_2, y_3 : \omega) \right] \right\} \mathrm{d}y_2\, \mathrm{d}y_3,
\end{aligned} \tag{B 4}$$

where the jump

$$\begin{aligned}
& \Delta \left[\frac{\partial}{\partial x_2} \bar{G}_{i2}(x_2, y_3 \,|\, x_2, x_3 : \omega, \omega/U(x_2)) \right] \\
& \quad \equiv \lim_{\varepsilon \to 0} \left[\frac{\partial}{\partial y_2} \bar{G}_2(y_2, y_3 \,|\, x_2, x_3 : \omega, \omega/U(y_2)) \Big|_{y_2 = x_2 + \varepsilon} \right] \\
& \qquad - \left[\frac{\partial}{\partial y_2} \bar{G}_2(y_2, y_3 \,|\, x_2, x_3 : \omega, \omega/U(y_2)) \Big|_{y_2 = x_2 - \varepsilon} \right]
\end{aligned} \tag{B 5}$$

will, in general, be non-zero. But this implies that

$$I_2 \to -\mathrm{e}^{\mathrm{i}\omega x_1/U(x_2)}\left[\frac{U^2(x_2)}{\omega x_1 U'(x_2)}\right]^2 \int_{-\infty}^{\infty} \Delta\left[\frac{\partial}{\partial x_2}\bar{G}_2(x_2, y_3 \,|\, x_2, x_3 : \omega, \omega/U(x_2))\right] \times \bar{\Omega}_c(x_2, y_3 : \omega)\,\mathrm{d}y_3 \tag{B 6}$$

as $x_1 \to -\infty$, since the method of stationary phase (Carrier, Krook & Pearson 1966, p. 274) (or continued integration by parts if there is no stationary phase point) can be used to show that the last term of (B 4) is $O(1/x_1^{5/2})$ in this limit.

Appendix C. Upstream behaviour of transverse particle displacement

We assume, for simplicity, that there is a one-to-one mapping $\boldsymbol{y}_T \to \{\eta(\boldsymbol{y}_T), \varsigma(\boldsymbol{y}_T)\}$ of the rectangular coordinate system $\boldsymbol{y}_T$ into an orthogonal coordinate system $\{\eta, \varsigma\}$ such that $U = U(\eta)$, and introduce this into the integral in (4.13) to obtain

$$\begin{aligned}
&\int_{A_T} \mathrm{e}^{\mathrm{i}\omega x_1/U(\boldsymbol{y}_T)} \frac{\bar{G}_i(\boldsymbol{y}_T \,|\, \boldsymbol{x}_T : \omega, \omega/U(\boldsymbol{y}_T))}{U(\boldsymbol{x}_T) - U(\boldsymbol{y}_T)} \bar{\Omega}_c(\boldsymbol{y}_T : \omega)\,\mathrm{d}\boldsymbol{y}_T \\
&= \int_{c_T}\left[\int_{\eta_0}^{\infty} \mathrm{e}^{\mathrm{i}\omega x_1/U(\eta)} \frac{\bar{G}_i(\eta, \varsigma \mid : \boldsymbol{x}_T, \omega, \omega/U(\eta))}{[U(\boldsymbol{x}_T) - U(\eta)]} \bar{\Omega}_c(\eta, \varsigma : \omega) \frac{\partial(y_2, y_3)}{\partial(\eta, \varsigma)}\,\mathrm{d}\eta\right]\mathrm{d}\varsigma \\
&= \int_{-\infty}^{\infty}\int_{c_T}\left[\int_{\eta_0}^{\infty} \mathrm{e}^{\mathrm{i}kx_1}\delta(k - \omega/U(\eta)) \frac{k\bar{G}_i(\eta, \varsigma \mid : \boldsymbol{x}_T, \omega, k)}{[kU(\boldsymbol{x}_T) - \omega]} \bar{\Omega}_c(\eta, \varsigma : \omega) \right. \\
&\quad \left. \times \frac{\partial(y_2, y_3)}{\partial(\eta, \varsigma)}\,\mathrm{d}\eta\right]\mathrm{d}\varsigma\,\mathrm{d}k \\
&= \lim_{n\to\infty}\lim_{\varepsilon\to 0}\int_{-\infty}^{\infty}\int_{c_T}\left[\int_{\eta_0}^{\infty} \mathrm{e}^{\mathrm{i}kx_1}\left(\frac{n}{\pi}\right)^{1/2} \mathrm{e}^{-n[k-(\omega+\mathrm{i}\varepsilon)/U(\eta)]^2} \right. \\
&\quad \left. \times \frac{k\bar{G}_i(\eta, \varsigma \mid : \boldsymbol{x}_T, \omega + \mathrm{i}\varepsilon, k)}{[kU(\boldsymbol{x}_T) - \omega - \mathrm{i}\varepsilon]} \bar{\Omega}_c(\eta, \varsigma : \omega + \mathrm{i}\varepsilon) \frac{\partial(y_2, y_3)}{\partial(\eta, \varsigma)}\,\mathrm{d}\eta\right]\mathrm{d}\varsigma\,\mathrm{d}k,
\end{aligned} \tag{C 1}$$

where $\partial(y_2, y_3)/\partial(\eta, \varsigma)$ denotes the Jacobian of the transform $\boldsymbol{y}_T \to \{\eta, \varsigma\}$, we have represented the delta function by a delta sequence (see Lighthill 1964, p. 17) and have written $U(\eta) \equiv U(\boldsymbol{y}_T(\eta))$, $\bar{G}_i(\eta, \varsigma \mid : \boldsymbol{x}_T, \omega, \omega/U(\eta)) \equiv \bar{G}_i(\boldsymbol{y}_T(\eta, \varsigma) \mid : \boldsymbol{x}_T, \omega, \omega/U(\eta))$ etc. Then, since $1/[kU(\boldsymbol{x}_T) - \omega - \mathrm{i}\varepsilon]$ is the only term that becomes infinite on the real k-axis when $\varepsilon = 0$, the limit can be made explicit everywhere else in the nth member of the sequence by setting $\varepsilon = 0$ there to obtain

$$\begin{aligned}
&\lim_{\varepsilon\to 0}\int_{-\infty}^{\infty}\int_{c_T}\left[\int_{\eta_0}^{\infty} \mathrm{e}^{\mathrm{i}kx_1}\left(\frac{n}{\pi}\right)^{1/2} \mathrm{e}^{-n[k-(\omega+\mathrm{i}\varepsilon)/U(\eta)]^2} \frac{k\bar{G}_i(\eta, \varsigma \mid : \boldsymbol{x}_T, \omega + \mathrm{i}\varepsilon, k)}{[kU(\boldsymbol{x}_T) - \omega - \mathrm{i}\varepsilon]} \right. \\
&\quad \left. \times\ \bar{\Omega}_c(\eta, \varsigma : \omega + \mathrm{i}\varepsilon) \frac{\partial(y_2, y_3)}{\partial(\eta, \varsigma)}\,\mathrm{d}\eta\right]\mathrm{d}\varsigma\,\mathrm{d}k \\
&= \lim_{\varepsilon\to 0}\int_{-\infty}^{\infty}\int_{c_T}\left[\int_{\eta_0}^{\infty} \mathrm{e}^{\mathrm{i}kx_1}\left(\frac{n}{\pi}\right)^{1/2} \mathrm{e}^{-n[k-\omega/U(\eta)]^2} \frac{k\bar{G}_i(\eta, \varsigma \mid : \boldsymbol{x}_T, \omega, k)}{[kU(\boldsymbol{x}_T) - \omega - \mathrm{i}\varepsilon]} \right. \\
&\quad \left. \times\ \bar{\Omega}_c(\eta, \varsigma : \omega) \frac{\partial(y_2, y_3)}{\partial(\eta, \varsigma)}\,\mathrm{d}\eta\right]\mathrm{d}\varsigma\,\mathrm{d}k.
\end{aligned} \tag{C 2}$$

The delta sequence limit can then be retaken to show that the singular integral in (4.13) can be interpreted in the following sense

$$\int_{A_T} \mathrm{e}^{\mathrm{i}\omega x_1/U(\boldsymbol{y}_T)} \frac{\bar{G}_i(\boldsymbol{y}_T \,|\, \boldsymbol{x}_T : \omega, \omega/U(\boldsymbol{y}_T))}{U(x_T) - U(\boldsymbol{y}_T)} \bar{\Omega}_c(\boldsymbol{y}_T : \omega)\, \mathrm{d}\boldsymbol{y}_T$$
$$= \frac{1}{U(\boldsymbol{x}_T)} \lim_{\bar{\varepsilon}\to 0} \int_{c_T} \left\{ \int_{\eta_0}^{\infty} \mathrm{e}^{\mathrm{i}\omega x_1/U(\eta)} \frac{U'(\eta) H(\eta, \varsigma \,|\, \boldsymbol{x}_T : \omega)}{[U^{-1}(\eta) - U^{-1}(\boldsymbol{x}_T) - \mathrm{i}\bar{\varepsilon}/\omega] U^2(\eta)} \,\mathrm{d}\eta \right\} \mathrm{d}\varsigma, \quad (\mathrm{C}\,3)$$

where we have put $\bar{\varepsilon} \equiv \varepsilon/U(\boldsymbol{x}_T)$ and

$$H(\eta, \varsigma \,|\, \boldsymbol{x}_T : \omega) \equiv \frac{U(\eta)\bar{G}_i(\eta, \varsigma \,|\, : \boldsymbol{x}_T, \omega, \omega/U(\eta))}{U'(\eta)} \bar{\Omega}_c(\eta, \varsigma : \omega) \frac{\partial(y_2, y_3)}{\partial(\eta, \varsigma)}. \quad (\mathrm{C}\,4)$$

But, as indicated in the introduction, our interest here is in the upstream behaviour of the solutions as $x_1 \to -\infty$. To this end we suppose, for definiteness, that the mean velocity profile has a single maximum, at say $\eta = \eta_{max}$, that $U = 0$ at the end points η_0, ∞ and that

$$\bar{\Omega}_c(y_2, y_3 : \omega) = O([U'(y_2)]^2) \quad \text{when } U'(y_2) \to 0. \quad (\mathrm{C}\,5)$$

(We shall verify that $\bar{\Omega}_c(y_2, y_3 : \omega)$ actually exhibits this behaviour after the fact.) Adding and subtracting terms to the particle displacement integral (C 1) then shows that

$$\int_{A_T} \mathrm{e}^{\mathrm{i}\omega x_1/U(\boldsymbol{y}_T)} \frac{\bar{G}_i(\boldsymbol{y}_T \,|\, \boldsymbol{x}_T : \omega, \omega/U(\boldsymbol{y}_T))}{U(\boldsymbol{x}_T) - U(\boldsymbol{y}_T)} \bar{\Omega}_c(\boldsymbol{y}_T : \omega)\, \mathrm{d}\boldsymbol{y}_T$$
$$= \frac{1}{U(\boldsymbol{x}_T)} \int_{c_T} \left\{ \int_{\eta_0}^{\eta_{max}} \mathrm{e}^{\mathrm{i}\omega x_1/U(\eta)} \frac{U'(\eta)[H(\eta, \varsigma \,|\, \boldsymbol{x}_T : \omega) - H(\bar{\eta}_1, \varsigma \,|\, \boldsymbol{x}_T : \omega)]}{[U^{-1}(\eta) - U^{-1}(\boldsymbol{x}_T)] U^2(\eta)} \,\mathrm{d}\eta \right.$$
$$\left. + \int_{\eta_{max}}^{\infty} \mathrm{e}^{\mathrm{i}\omega x_1/U(\eta)} \frac{U'(\eta)[H(\eta, \varsigma \,|\, \boldsymbol{x}_T : \omega) - H(\bar{\eta}_2, \varsigma \,|\, \boldsymbol{x}_T : \omega)]}{[U^{-1}(\eta) - U^{-1}(\boldsymbol{x}_T)] U^2(\eta)} \,\mathrm{d}\eta \right\} \mathrm{d}\varsigma$$
$$- \frac{1}{U(\boldsymbol{x}_T)} \int_{c_T} [H(\bar{\eta}_1, \varsigma \,|\, \boldsymbol{x}_T : \omega) - H(\bar{\eta}_2, \varsigma \,|\, \boldsymbol{x}_T : \omega)] \,\mathrm{d}\varsigma$$
$$\times \left\{ \lim_{\bar{\varepsilon}\to 0} \int_a^{\infty} \frac{\mathrm{e}^{\mathrm{i}\omega x_1/U}}{[U^{-1} - U^{-1}(\boldsymbol{x}_T) - \mathrm{i}\bar{\varepsilon}/\omega]} \,\mathrm{d}\left(\frac{1}{U}\right) \right\}, \quad (\mathrm{C}\,6)$$

where $a \equiv 1/U(\eta_{max})$, and $\bar{\eta}_j$ for $j = 1, 2$ are the roots of $U(\bar{\eta}_j) = U(\boldsymbol{x}_T)$ with $U'(\bar{\eta}_1) < 0$.

But dividing the range of integration into two parts, changing integration variables and noting that the final contour integral must be closed in the lower half-plane for $x_1 < 0$ shows that

$$\lim_{\bar{\varepsilon}\to 0} \int_a^{\infty} \frac{\mathrm{e}^{\mathrm{i}\omega x_1 [U^{-1} - U^{-1}(\boldsymbol{x}_T)]}}{[U^{-1} - U^{-1}(\boldsymbol{x}_T) - \mathrm{i}\bar{\varepsilon}/\omega]} \,\mathrm{d}\left(\frac{1}{U}\right)$$
$$= \lim_{\bar{\varepsilon}\to 0} \left\{ \int_{-b(\boldsymbol{x}_T)\omega x_1}^{\infty \operatorname{sgn}\omega} \frac{\mathrm{e}^{\mathrm{i}t}}{t - \mathrm{i}\bar{\varepsilon} x_1} \,\mathrm{d}t + \mathrm{e}^{-\mathrm{i}\omega x_1/U(\boldsymbol{x}_T)} \int_{-\infty \operatorname{sgn}\omega}^{\infty \operatorname{sgn}\omega} \frac{\mathrm{e}^{\mathrm{i}\tau x_1}}{\tau - \mathrm{i}\bar{\varepsilon}} \,\mathrm{d}\tau \right\}$$
$$= \lim_{\bar{\varepsilon}\to 0} \left\{ \int_{-b(\boldsymbol{x}_T)\omega x_1}^{\infty \operatorname{sgn}\omega} \frac{\mathrm{e}^{\mathrm{i}t}}{t - \mathrm{i}\bar{\varepsilon} x_1} \,\mathrm{d}t + \mathrm{e}^{-\mathrm{i}\omega x_1/U(\boldsymbol{x}_T)} \operatorname{sgn}\omega \int_{-\infty}^{\infty} \frac{\mathrm{e}^{\mathrm{i}\tau x_1}}{\tau - \mathrm{i}\bar{\varepsilon}} \,\mathrm{d}\tau \right\} \to 0,$$
$$\text{as } x_1 \to -\infty, \quad (\mathrm{C}\,7)$$

where $b(\boldsymbol{x}_T) \equiv [U(\boldsymbol{x}_T)]^{-1} - a > 0$. And since the integrands of the inner integrals in the first term on the right-hand side of (C 6) are now finite at $\boldsymbol{y}_T = \boldsymbol{x}_T$, the first of these can be integrated by parts from η_0 to $\bar{\eta}_1$ and from $\bar{\eta}_1$ toη_{max} to obtain

$$\frac{1}{U(\boldsymbol{x}_T)}\int_{\eta_0}^{\eta_{max}} \mathrm{e}^{\mathrm{i}\omega x_1/U(\eta)}\frac{U'(\eta)[H(\eta,\varsigma\,|\,\boldsymbol{x}_T:\omega)-H(\bar{\eta}_1,\varsigma\,|\,\boldsymbol{x}_T:\omega)]}{[U^{-1}(\eta)-U^{-1}(\boldsymbol{x}_T)]U^2(\eta)}\,\mathrm{d}\eta$$
$$= -\frac{1}{\mathrm{i}\omega x_1}\mathrm{e}^{\mathrm{i}\omega x_1/U(\bar{\eta}_1)}\;\Delta\left[\frac{\partial\bar{G}_2(\eta,\varsigma\,|\;:\boldsymbol{x}_T,\omega,\omega/U(\eta))}{\partial\eta}\right]\Bigg|_{\eta=\bar{\eta}_1}$$
$$\times\left\{\frac{\bar{\Omega}_c(\eta,\varsigma:\omega)\dfrac{\partial(y_2,y_3)}{\partial(\eta,\varsigma)}}{[U'(\eta)]^2}\right\}_{\eta=\bar{\eta}_1}$$
$$-\frac{1}{\mathrm{i}\omega x_1}\int_{\eta_0}^{\eta_{max}}\mathrm{e}^{\mathrm{i}\omega x_1/U(\eta)}\frac{\partial}{\partial\eta}\left\{\frac{[H(\eta,\varsigma\,|\,\boldsymbol{x}_T:\omega)-H(\bar{\eta}_1,\varsigma\,|\,\boldsymbol{x}_T:\omega)]}{[U(\boldsymbol{x}_T)-U(\eta)]U(\eta)}\right\}\mathrm{d}\eta, \quad (\mathrm{C}\,8)$$

where $\Delta[\partial\bar{G}_2(\eta,\varsigma|:\boldsymbol{x}_T,\omega,\omega/U(\eta))/\partial\eta]|_{\eta=\bar{\eta}_1}$ denotes the jump in $\partial\bar{G}_2(\eta,\varsigma|:\boldsymbol{x}_T,\omega,\omega/U(\eta))/\partial\eta$ at $\eta=\bar{\eta}_1$, while the second of these can be integrated by parts from η_{max} to $\bar{\eta}_2$ and from $\bar{\eta}_2$ to ∞, to obtain a similar result and thereby show that this term is $O(1/x_1)$ as $x_1 \to -\infty$, and, therefore, that $\bar{\eta}_\perp$ satisfies (4.14).

REFERENCES

Afsar, M. Z., Leib, S. J. & Bozak, R. F. 2017 Effect of de-correlating turbulence on the low frequency decay of jet–surface interaction noise in sub-sonic unheated air jets using a CFD-based approach. *J. Sound Vib.* **386** (6), 177–207.

Afsar, M. Z., Sescu, A. & Leib, S. J. 2016 Predictive capability of low frequency jet noise using an asymptotic theory for the adjoint vector Green's function in non-parallel flow. AIAA Aero-acoustics. *AIAA Paper* 2016-2804.

Ayton, L. J., Gill, J. & Peake, N. 2016 The importance of the unsteady Kutta condition when modelling gust–aerofoil interaction. *J. Sound Vib.* **378**, 28–37.

Batchelor, G. K. & Proudman, I. 1954 The effect of rapid distortion of a fluid in turbulent motion. *Q. J. Mech. Appl. Maths* **7** (1), 83–103.

Bers, A. 1975 Linear waves and instabilities. In *Plasma Physics* (ed. C. Dewitt & J. Perraud), pp. 113–216. Gordon & Breach.

Bridges, J. 2014 Noise from Aft Deck Exhaust Nozzles – differences in experimental embodiments. In *52nd AIAA Aerospace Sciences Meeting – 13–17 January 2014, Nat'l Harbor, MD*.

Bridges, J. & Brown, C. A. 2005 Validation of the small hot jet rig for jet noise research. *AIAA Paper* 2005-2846.

Bridges, J., Brown, C. A. & Bozak, R. 2014 Experiments on exhaust of tightly integrated propulsion systems. *AIAA Paper* 2014-2904.

Briggs, R. J. 1964 *Electron Stream Interaction with Plasmas*. MIT Press.

Brinkman, K. W. & Walker, J. D. A. 2001 Instabilities in a viscous flow driven by streamwise vortices. *J. Fluid Mech.* **432**, 127–166.

Brown, C. 2012 Jet–surface interaction test: far-field noise results. *ASME Paper* GT2012-69639.

Brown, C. A. 2015 An empirical jet–surface interaction noise model with temperature and nozzle aspect ratio effects. In *53rd AIAA Aerospace Sciences Meeting*.

Brown, C. A. & Bridges, J. 2006 Small hot jet acoustic rig validation. *NASA-TM*-2006-214234.

Brown, S. N. & Daniels, P. G. 1975 On the viscous flow about the trailing edge of a rapidly oscillating plate. *J. Fluid Mech.* **67** (4), 743–761.

CARRIER, G. F., KROOK, M. & PEARSON, C. E. 1966 *Functions of a Complex Variable*. McGraw-Hill.

CASSEL, K. W. & CONLISK, A. T. 2014 Unsteady separation in vortex induced boundary layers. *Phil. Trans. R. Soc. Lond.* **372** (2020), 20130348.

CHINAUD, M., ROUCHON, J. F., DUHAYON, E., SCHELLER, J., CAZIN, S., MARCHAL, M. & BRAZA, M. 2014 Trailing-edge dynamics and morphing of a deformable flat plate at high Reynolds number by time-resolved PIV. *J. Fluids Struct.* **47**, 41–54.

COWLEY 2001 Laminar boundary layer theory: a 20th century paradox? In *Proc. ICTM 2000, Chicago, IL, August–September 2000*, pp. 389–411. Kluwer.

CRIGHTON, D. G. 1985 The Kutta condition in unsteady flow. *Annu. Rev. Fluid Mech.* **17**, 411–445.

DOWLING, A. P., FFOWCS WILLIAMS, J. E. & GOLDSTEIN, M. E. 1978 Sound propagation in a moving stream. *Phil. Trans. R. Soc. Lond.* A **288**, 321–349; **40**, 657–670.

DRAZIN, P. G. & REID, W. H. 1981 *Hydrodynamic Stability*. Cambridge University Press.

GOLDSTEIN, M. E. 1978*a* Unsteady vortical and entropic distortions of potential flows round arbitrary obstacles. *J. Fluid Mech.* **89**, 433–468.

GOLDSTEIN, M. E. 1978*b* Characteristics of the unsteady motion on transversely sheared mean flows. *J. Fluid Mech.* **84** (2), 305–329.

GOLDSTEIN, M. E. 1979*a* Turbulence generated by entropy fluctuation with non-uniform mean flows. *J. Fluid Mech.* **93** (2), 209–224.

GOLDSTEIN, M. E. 1979*b* Scattering and distortion of the unsteady motion on transversely sheared mean flows. *J. Fluid Mech.* **91** (4), 601–632.

GOLDSTEIN, M. E. 2005 On identifying the true sources of aerodynamic sound. *J. Fluid Mech.* **526**, 337–347.

GOLDSTEIN, M. E. 2009 A theoretical basis for identifying the sound sources in a turbulent flow. *Intl J. Aeroacoust.* **8** (4), 283–300.

GOLDSTEIN, M. E., AFSAR, M. Z. & LEIB 2013*a* Non-homogeneous rapid distortion theory on transversely sheared mean flows. *J. Fluid Mech.* **736**, 532–569.

GOLDSTEIN, M. E., AFSAR, M. Z. & LEIB 2013*b* Structure of small amplitude motion on transversely sheared mean flows. *NASA/TM*-2013-217862.

GRADSHTEYN, I. S. & RYSHIK, I. M. 1965 *Table of Integrals, Series and Products*. Academic.

HUNT, J. C. R. 1973 A theory of turbulent flow around two dimensional bluff bodies. *J. Fluid Mech.* **61**, 625–706.

HUNT, J. C. R., ISHIHARA, T., SZUBERT, D., ASPROULIAS, I., HOARAU, Y. & BRAZA, M. 2016 Turbulence near interfaces – modelling and simulations. In *Advances in Fluid–Structure Interaction*, pp. 283–292. Updated contributions reflecting new findings presented at the *ERCOFTAC Symposium on Unsteady Separation in Fluid–Structure Interaction, 17–21 June 2013, St John Resort, Mykonos, Greece*. Springer.

KHAVARAN, A., BOZAK, R. F. & BROWN, C. A. 2016 Jet surface interaction noise in a planar exhaust. *AIAA Paper* 2016-2863.

KOVASZNAY, L. S. G. 1953 Turbulence in supersonic flow. *J. Aero Sci.* **20** (10), 657–674.

LEIB, S. J. & GOLDSTEIN, M. E. 2011 Hybrid source model for predicting high-speed jet noise. *AIAA J.* **49** (7), 1324–1335.

LIGHTHILL, M. J. 1964 *Fourier Analysis and Generalized Functions*. Cambridge University Press.

LIVESCU, D. & MADNIA, C. K. 2004 Small scale structure of homogenious turbulent shear flow. *Phys. Fluids* **16** (8), 2864–28787.

MANI, R. 1976 Influence of jet flow on jet noise. *J. Fluid Mech.* **173**, 753–793.

MOFFATT, H. K. 1967 Interaction of turbulence with strong wind shear. In *Colloquium on Atmospheric Turbulence and Radio Wave Propagation* (ed. A. M. Yaglom & V. I. Tatarski), pp. 139–156. Nauka.

MÖHRING, W. 1976 Über Schallwellen in Scherströmungen, Fortschritte der Akustik. *DAGA* 76 VDI, pp. 543–546.

MOORE, F. K. 1954 Unsteady oblique interaction of a shock wave with a plane disturbance. *NACS Tech. Rep.* 2879.

ORR, W. 1907 The stability and instability of the steady motions of a perfect liquid and of a viscous liquid. *Proc. R. Irish Acad.* A **27**, 9–68, 69–138.

RIBNER, H. S. 1953 Convection of a pattern of vorticity through a shock wave. *NACA Tech. Rep.* 1164.

SAGAUT, P. & CAMBON, C. 2008 *Homogeneous Turbulence Dynamics*. Cambridge University Press.

SEARS, W. R. 1941 Some aspects of non-stationary airfoil theory and its practical application. *J. Aero. Sci.* **8** (3), 104–108.

TAYLOR, G. I. 1935 Turbulence in a contracting stream. *Z. Angew. Math. Mech.* **15**, 91–96.

WIENER, N. 1938 The use of statistical theory to study turbulence. In *Proc. 5th Int. Congress Appl. Mech.*, pp. 356–360. Wiley.

XIE, Z., KARIMI, M. & GIRIMAJI, S. S. 2017 Small perturbation evolution in compressible Poiseulle flow–velocity interactions and obliqueness effects. *J. Fluid Mech.* **814**, 249–276.

ZAMAN, K., BROWN, C. A. & BRIDGES, J. E. 2013 Interaction of a rectangular jet with a flat-plate placed parallel to the flow. *AIAA Paper* 2013-2184. *NASA/TM*-2013-217879 (E-18684).